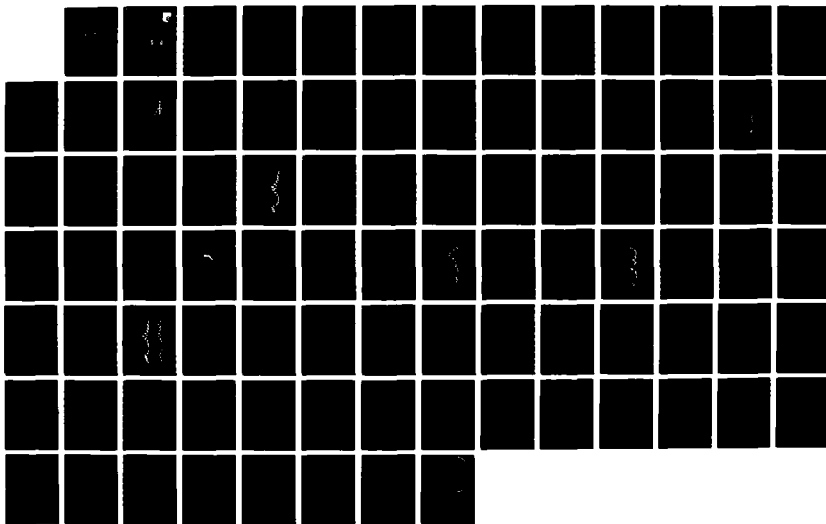AD-A184 457    NITROGEN ENERGY TRANSFER STUDY(U) SYSTEMS RESEARCH LABS    1/1
INC DAYTON OH RESEARCH APPLICATIONS DIV   D F GROSJEAN
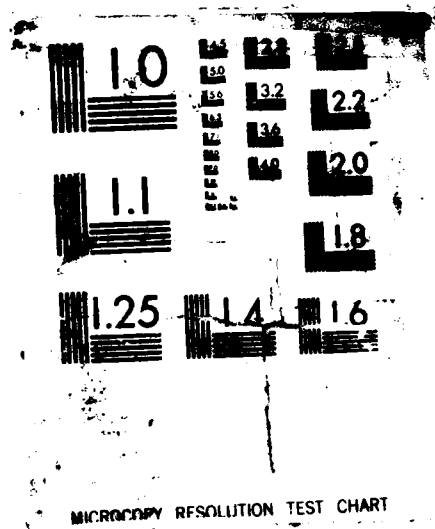AUG 87 AFWAL-TR-87-2038 F33615-84-C-2441

UNCLASSIFIED                                          F/G 7/4        NL

MICROCOPY RESOLUTION TEST CHART

AFWAL-TR-87-2038
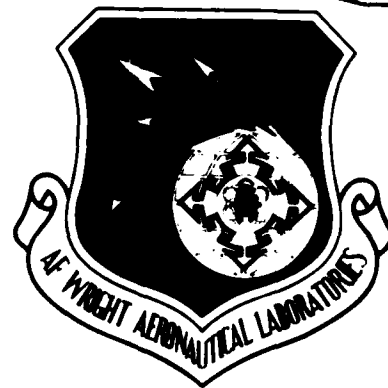
AD-A184 457

NITROGEN ENERGY TRANSFER STUDY

D. F. GROSJEAN

Research Applications Division
Systems Research Laboratories, Inc.
2800 Indian Ripple Road
Dayton, OH 45440-3696

August 1987

DTIC
SELECTED
SEP 1 0 1987
D

Final Report for Period 10 September 1984 - 31 December 1986

Approved for public release; distribution is unlimited.

AERO PROPULSION LABORATORY
AIR FORCE WRIGHT AERONAUTICAL LABORATORIES
AIR FORCE SYSTEMS COMMAND
WRIGHT-PATTERSON AIR FORCE BASE, OH 45433-6563

87 9 9 102

## NOTICE

When Government drawings, specifications, or other data are used for any purpose other than in connection with a definitely Government-related procurement, the United States Government incurs no responsibility or any obligation whatsoever. The fact that the Government may have formulated or in any way supplied the said drawings, specifications, or other data, is not to be regarded by implication, or otherwise in any manner construed, as licensing the holder, or any other person or corporation; or as conveying any rights or permission to manufacture, use, or sell any patented invention that may in any way be related thereto.

This report has been reviewed by the Office of Public Affairs (ASD/PA) and is releasable to the National Technical Information Service (NTIS). At NTIS, it will be available to the general public, including foreign nations.

This technical report has been reviewed and is approved for publication.


PETER BLETZINGER, Project Engineer
Power Components Branch
Aerospace Power Division
Aero Propulsion Laboratory

PAUL R. BERTHEAUD, Chief
Power Components Branch
Aerospace Power Division
Aero Propulsion Laboratory


FOR THE COMMANDER


JAMES D. REAMS
Chief, Aerospace Power Division
Aero Propulsion Laboratory


If your address has changed, if you wish to be removed from our mailing list, or if the addressee is no longer employed by your organization please notify AFWAL/POOC-3, Wright-Patterson AFB, OH 45433-6563 to help us maintain a current mailing list.

Copies of this report should not be returned unless return is required by security considerations, contractual obligations, or notice on a specific document.

$AD A 184 959$

# REPORT DOCUMENTATION PAGE

| 1a. REPORT SECURITY CLASSIFICATION<br>Unclassified | | 1b. RESTRICTIVE MARKINGS |
|---|---|---|
| 2a. SECURITY CLASSIFICATION AUTHORITY | | 3. DISTRIBUTION/AVAILABILITY OF REPORT |
| 2b. DECLASSIFICATION/DOWNGRADING SCHEDULE | | Approved for public release; distribution is unlimited. |
| 4. PERFORMING ORGANIZATION REPORT NUMBER(S)<br>6846 Final | | 5. MONITORING ORGANIZATION REPORT NUMBER(S)<br>AFWAL-TR-87-2038 |

| 6a. NAME OF PERFORMING ORGANIZATION<br>Systems Research Laboratories, Inc. | 6b. OFFICE SYMBOL<br>(If applicable) | 7a. NAME OF MONITORING ORGANIZATION<br>Aero Propulsion Laboratory (AFWAL/POOC-3)<br>Air Force Wright Aeronautical Laboratories |
|---|---|---|
| 6c. ADDRESS (City, State and ZIP Code)<br>2800 Indian Ripple Road<br>Dayton, OH 45440-3696 | | 7b. ADDRESS (City, State and ZIP Code)<br>Wright-Patterson AFB, OH 45433-6563 |
| 8a. NAME OF FUNDING/SPONSORING ORGANIZATION | 8b. OFFICE SYMBOL<br>(If applicable) | 9. PROCUREMENT INSTRUMENT IDENTIFICATION NUMBER<br>F33615-84-C-2441 |

| 8c. ADDRESS (City, State and ZIP Code) | 10. SOURCE OF FUNDING NOS. | | | |
|---|---|---|---|---|
| | PROGRAM ELEMENT NO.<br>61102F | PROJECT NO.<br>2301 | TASK NO.<br>S2 | WORK UNIT NO.<br>33 |

11. TITLE (Include Security Classification)
Nitrogen Energy Transfer Study (Unclass.)

12. PERSONAL AUTHOR(S)
Grosjean, D. F.

| 13a. TYPE OF REPORT<br>Final Report | 13b. TIME COVERED<br>FROM 84-09-10 TO 86-12-31 | 14. DATE OF REPORT (Yr., Mo., Day)<br>August 1987 | 15. PAGE COUNT<br>90 |
|---|---|---|---|

16. SUPPLEMENTARY NOTATION

| 17. COSATI CODES | | | 18. SUBJECT TERMS (Continue on reverse if necessary and identify by block number) |
|---|---|---|---|
| FIELD | GROUP | SUB. GR. | Nitrogen Afterglow, Nitrogen Metastable, Nitrogen Spectroscopy, Dielectric-Barrier Discharge, Surface-Wave Discharge |
| 07 | 04 | | |

19. ABSTRACT (Continue on reverse if necessary and identify by block number)

The use of $N_2$ as an energy-transfer medium between an electrical discharge and a target molecule was investigated experimentally. Efforts were concentrated primarily upon the attainment of a high density of $N_2(A^3\Sigma_u^+)$ metastable molecules in a flowing afterglow arrangement. Excitation techniques utilized were microwave surface-wave discharges and dielectric-barrier discharges at pressures of 3 - 760 Torr in $N_2$ and $Ar/N_2$ mixtures. Although the radiative lifetime of $N_2(A)$ is long, the effective lifetime at high pressures was found to be much too short for use in a flowing system. The only long-lived species present at significant densities in the afterglow was $N(^4S)$ atoms.

| 20. DISTRIBUTION/AVAILABILITY OF ABSTRACT | 21. ABSTRACT SECURITY CLASSIFICATION |
|---|---|
| UNCLASSIFIED/UNLIMITED ☐ SAME AS RPT. ☒ DTIC USERS ☐ | Unclassified |

| 22a. NAME OF RESPONSIBLE INDIVIDUAL<br>Peter Bletzinger, Ph.D. | 22b. TELEPHONE NUMBER (Include Area Code)<br>(513) 255-2923 | 22c. OFFICE SYMBOL<br>AFWAL/POOC-3 |
|---|---|---|

**DD FORM 1473, 83 APR**   EDITION OF 1 JAN 73 IS OBSOLETE

## Preface

This report covers work performed during the period 10 September 1984 through 31 December 1986 under Contract F33615-84-C-2441 (Project 2301, Task S2) by the Research Applications Division of Systems Research Laboratories, Inc., 2800 Indian Ripple Road, Dayton, OH 45440-3696. The contract was administered under the direction of the Air Force Wright Aeronautical Laboratories, Aero Propulsion Laboratory (AFWAL/POOC-3), Wright-Patterson Air Force Base, OH 45433-6563, with Dr. P. Bletzinger acting as the Government Project Monitor.

The author wishes to acknowledge the technical assistance of M. Rowe and B. Sarka of SRL and helpful discussions with G. E. Caledonia, B. D. Green, and L. G. Piper of Physical Sciences, Inc. Also appreciated were the discussions with and cooperation of members of the AFWAL Aero Propulsion Laboratory. The editorial assistance of M. Whitaker in preparation of this report is grately appreciated.

| Accesion For | | |
|---|---|---|
| NTIS CRA&I | ☑ | |
| DTIC TAB | ☐ | |
| Unannounced | ☐ | |
| Justification | | |
| By | | |
| Distribution / | | |
| Availability Codes | | |
| Dist | Avail and / or Special | |
| A-1 | | |

iii

## TABLE OF CONTENTS

## LIST OF ILLUSTRATIONS

## LIST OF ILLUSTRATIONS (Continued)

## LIST OF ILLUSTRATIONS (Concluded)

## Section I
## INTRODUCTION

Numerous methods of creating "active" nitrogen have been reported in the literature (see Refs. 1 and 2, for example), although the majority of the work has been performed at low gas pressures (< 20 Torr). The purpose of the effort described here was to determine experimentally the feasibility of producing a high density of metastable states of $N_2$ in an afterglow arrangement suitable for transfer of the stored energy to a lasant species.

The species responsible for the high degree of reactivity of an $N_2$ afterglow are vibrationally and electronically excited $N_2$ molecules as well as ground and excited states of atomic N. The term "Lewis-Rayleigh afterglow" is used to describe the persistent radiation emitted by $N_2$ after the excitation source is removed. It consists primarily of the first-positive bands ($B^3\Pi_g - A^3\Sigma_u^+$) but also includes numerous other radiative transitions (see Ref. 1 for complete description).

Of major interest is the lowest-lying electronic state of $N_2(A^3\Sigma_u^+)$ because of its long radiative lifetime ($\sim$ 2 sec),[2-4] its relatively high internal energy (6.17 eV for v = 0),[5] and its large cross section for energy transfer to other molecules.[6-8] The promise of efficient, fast energy transfer to NO and subsequent radiation of the NO $\gamma$-bands (NO $B^2\Pi \rightarrow X^2\Pi$) has resulted in interest in the possibility of an $NO/N_2$ tunable light source. However, reactions of other excited $N_2$ states as well as N-atoms with NO (or other target gas) makes it necessary that the excitation method favor the formation of $N_2$(A) while minimizing the formation of competing states. In addition, in order to attain a significant light flux, a large density of excited states must exist.

For attaining a large excited-state density, use of high pressures (100 - 760 Torr) is seemingly preferable to attempting excitation of a high percentage of a low-pressure gas. Since only electrical-discharge excitation was considered for this effort, two promising techniques were studied--microwave surface-wave excitation and dielectric-barrier discharge excitation.

1

Section II contains the background for selection of these two techniques. Sections III and IV describe the details of the microwave studies and application of the dielectric-barrier discharge, respectively. The diagnostic techniques pertinent to measurement of excited states are discussed in Section V, and experimental equipment developed for this effort are described in Section VI.

## Section II
## BACKGROUND

Electrical-discharge pumping of a gas involves a transfer of energy from an electric (or magnetic) field to charged particles which, in turn, transfer energy in collision with neutral gas molecules. The large energy-transfer cross sections for low-energy electrons in $N_2$ generally result in large fractions of the total energy input going into vibrational excitation in a pure $N_2$ discharge.[9]

The metastable nature of the symmetric $N_2$ molecule, then, results in a significant amount of energy being converted to gas heating rather than atomic-state excitation. The absence of electron-attachment processes in pure $N_2$ results in a relatively low electric field and, consequently, a low average electron temperature after the discharge is established.[9] A DC discharge is, therefore, not attractive for the generation of the $N_2(A)$ state unless electron diffusion losses can be made large. A small-bore "capillary" arrangement enhances the diffusion losses, but the large amount of heat and high electrode-erosion create difficulties in achieving an acceptable discharge in practice.

The high-pressure pulsed discharge will provide sufficiently hot electrons for atomic-state pumping only during the short ($\sim$ 10 nsec) over-voltage phase of the discharge cycle. However, unless the discharge is terminated as the E/N and electron temperature drop, much of the total energy will be channeled into vibrational energy, as discussed above. Providing a sufficiently short (temporal) electrical pulse is impractical.[10] In addition, the amount of energy deposited during the over-voltage phase is small due to the low electron density. A high repetition rate would, therefore, be required if significant energy transfer were desired. Thus, the standard configuration of a pulsed discharge with integral metal electrodes would not be efficient in producing large concentrations of $N_2$ metastables.

However, the insertion of a dielectric between the gas and at least one electrode will result in rapid termination of the discharge as the electron density builds up. This is the principle behind the "ozonizer"

3

discharge--also referred to as a silent discharge, dielectric discharge, or dielectric-barrier discharge--used commonly for production of ozone from atmospheric-pressure oxygen or air.[11-13] The requirements for generating atomic O from $O_2$ for subsequent formation of $O_3$ are similar to those for direct electron-excitation of $N_2$. That is, the two major dissociating states of $O_2$ have thresholds[12] at $\sim$ 6 eV and $\sim$ 8.4 eV; the threshold of the $N_2(A)$ state is 6.17 eV.[5] This discharge technique has been reportedly used successfully for production of $N_2(A)$ at 1 - 20 Torr pressure[14,15] and at atmospheric pressure where large concentrations appeared feasible.[16,17]

The use of a dielectric barrier at both electrodes would aid in maintaining the cleanliness of the gas. This "dielectric-barrier" (preferred term) discharge arrangement, then, appears to be one of the most promising techniques for generation of large $N_2(A)$ concentrations in the present contractual effort. For a small electrode gap (1 - 3 mm), the required discharge voltage should be $\leq$ 10 kV (based on $O_3$ generation data); therefore, high-frequency (1 - 10 kHz), solid-state drivers are feasible as power sources.

Microwave and RF excitation is used frequently for generation of active nitrogen.[1] Generally the most prominent emission observed is the first-positive band system, indicating a large concentration of atomic N. At very low pressure ($\leq$ 1 Torr), two-body recombination of N-atoms occurs while three-body processes appear to dominate at pressures above $\sim$ 1 Torr.[18,19] A typical microwave discharge (pressures $\leq$ 10 Torr) produces large amounts of atomic N and is often used as a source of dissociated nitrogen (e.g., Refs. 20, 21). In a CW microwave discharge, one would expect the electron energy distribution to be somewhat similar to the DC discharge discussed earlier, that is, a relatively low average electron temperature and a large amount of vibrational excitation and resulting high gas temperature. It appears, then, that the $N_2(A)$-state kinetics are dominated by the N-atom concentration--both production and loss channels. This limits the maximum achievable $N_2(A)$ density.[15] Assuming a three-body N-atom recombination-rate coefficient[19] of $10^{-31}$ $cm^6$ $sec^{-1}$ and a destruction-rate coefficient[20] of 5 x $10^{-11}$ $cm^3$ $sec^{-1}$, a saturation density of $\sim 10^{-3}$ x N-atom concentration is calculated for a

10-Torr discharge. The dominant reactive species in the near afterglow, therefore, will be N-atoms, rather than the desired molecular meta-stable. One cannot dismiss reactions involving other excited states[22] of $N_2$, but it appears that a low-pressure microwave discharge will generate large N-atom concentrations.

As $N_2$ pressure is increased, it becomes exceedingly difficult to main-tain a volume discharge with microwave excitation. However, successful RF and microwave excitation at atmospheric pressure has been reported in a surface-wave configuration.[23-27] Because the discharge excitation occurs only near the dielectric surface, the diffusion losses of elec-trons will be larger, possibly resulting in a higher electron tempera-ture than that found in the volume microwave configuration discussed above.

An attractive alternative to direct microwave excitation of $N_2$ is RF/microwave excitation of Ar to form the rare-gas metastables (11.55 and 11.72 eV),[28] followed by collisional transfer of energy to form $N_2$ elec-tronically excited molecules without effecting significant dissocia-tion.[29,30] The use of Kr and Xe metastables should also produce the $N_2(A)$, but their cost would inhibit their usefulness in fast-flow sys-tems. Typically, this technique is applied at low pressure, but the surface-wave applicator has been shown to be very useful for rare-gas excitation at atmospheric pressure.

Another method of producing $N_2(A)$ molecules is the e-beam-sustained dis-charge configuration. Results of a theoretical investigation[31] showed that a significant $N_2(A)$ concentration was achievable for E/N sustainer fields $\geq$ 40 Td. Unfortunately, fields of $\geq$ 10 Td cannot be attained--due to arcing--at high pressures in the present AFWAL e-beam test cell.[32]

In summary, the two most promising techniques of producing a large $N_2(A)$ metastable density without significant $N(^4S)$ atom concentration are the dielectric-barrier and the RF/microwave surface-wave configurations.

Although a great deal of information concerning $N_2$ discharges and after-glows can be found in the literature, it is often contradictory. The large number of electronic states, many having similar internuclear vibrational end points, and the metastable nature of vibrational states result in inconsistent interpretations of kinetic effects. The potential-energy curves of Fig. 1 show the complicated nature of this molecule. In addition, the sensitivity of the electronic excited-state population to impurities often results in inconsistent experimental results. The review by Wright and Winkler[1] summarizes the understarding of the $N_2$ molecule up to 1968. In 1973 Golde and Thrush[33] published an excellent overview of the understanding of the afterglow kinetics. The most recent review of spectroscopic data can be found in Lofthus and Krupenie.[2]

$N_2$ afterglows can be placed in two categories--short-lived and long-lived. The long-lived glow, known as the Lewis-Rayleigh afterglow, is characterized by a dominance of visible emission of the first-positive bands ($B^3\pi_g^+ - A^3\Sigma_u^+$), usually with B-state vibrational levels (v') of 0 - 12 present. The short-lived auroral and "pink" afterglows are char-acterized by dominant emission from not only the first-positive but also the second-positive ($C^3\pi_u - B^3\pi_g$) and the first-negative ($N_2^+ B^3\Sigma_u^+ - X^2\Sigma_g^+$) bands.

In addition to the B-state emission, radiation from $A^3\Sigma_u^+$, $a'^1\Sigma_u^-$, $a^1\pi_g$, and $B'^3\Sigma_u^-$ as well as $N(^2D)$ and $N(^2P)$ have been observed in the Lewis-Rayleigh afterglow. Although emission from the $^5\Sigma_g^+$, $w^1\Delta_u$, and high vibrational levels of the $A^3\Sigma_u^+$ and $a'^1\Sigma_u^-$ have not been observed, these states are postulated to exist in these afterglows in order to explain the observed vibrational distribution of the emitting states.[33] The recently measured[34-48] effects of the $W^3\Delta_u$ have established parameters of this electronic state also.

The source of the long-lived Lewis-Rayleigh afterglow has been shown rather conclusively to be $N(^4S)$ atoms,[33] although an exact mechanism has not yet been universally accepted. Generally, either three-body inverse pre-dissociation via the very shallow $^5\Sigma_g$ state[19,39] or three-body relaxation into very high vibrational levels[33,40] of the $A^3\Sigma_u^+$ is

6
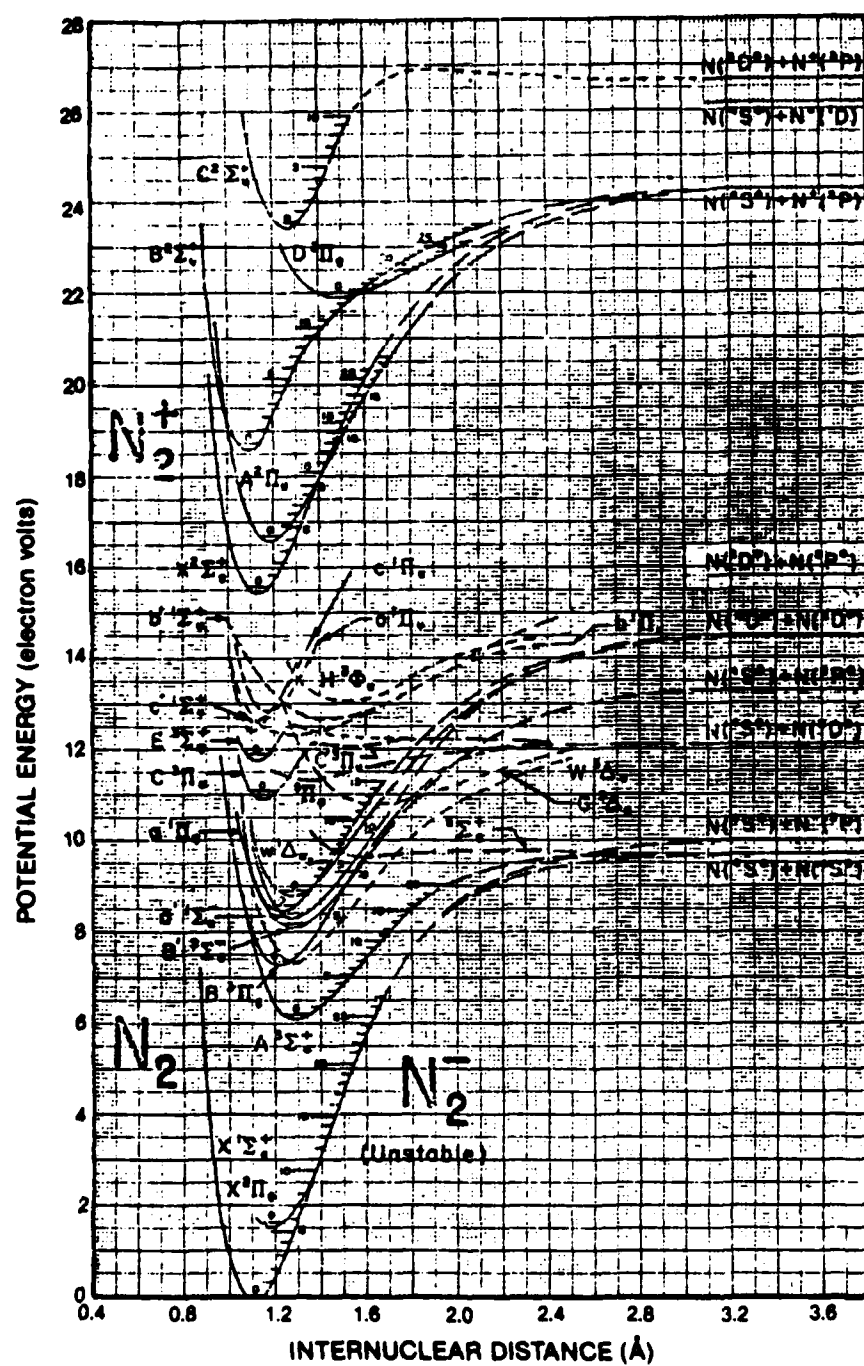
Figure 1. Potential Energy Curves for $N_2$ and $N_2^+$ (from Ref. 2).

accepted. Both theories invoke the unbound states of the $^5\Sigma_g$ as the original precursor. Despite the mechanism involved, it is apparent that discharge-created $N(^4S)$ is responsible for initiation of the long-lived glow.

As mentioned above, the $N(^4S)$ quenches the $N_2(A)$ so efficiently that large concentrations of the $N_2(A)$ metastable via the N-atom recombination channel are not feasible. Caledonia, et al.,[41] calculate a maximum concentration of $N_2(A)$ of $10^{12}$ cm$^{-3}$ when N-atom recombination is the source of excited states in an afterglow. Therefore, the common Lewis-Rayleigh afterglow is not amenable to the present goal of large concentrations of electronically excited, metastable $N_2$ molecules.

The "pink" afterglow,[42-44] however, which is readily produced in a low-pressure clean laboratory system, exhibits emission from states having internal energies as high as 19.9 eV. This short-lived afterglow is characterized by a dark region between the discharge glow and a pinkish-white glow which begins $\sim$ 10 msec downstream and lasts 5 - 20 msec, often exhibiting oscillatory behavior in intensity downstream.

Early attempts to explain the mechanism of the pink afterglow were concentrated on identifying highly excited metastables exiting the discharge.[44,45] Subsequent ultraviolet-absorption measurements of Bass[46] and Tanaka, et al.,[47] showed the presence of very high vibrational levels of $N_2(X)$; levels of up to v" = 25 were observed. The presence of these levels upstream and into the glow region and the decrease in their population downstream of the glow led Tanaka, et al.,[47] to the conclusion that while the vibrational metastables cannot directly account for the high electronic states, they are a necessary constituent to the pink-afterglow kinetics. Lund and Oskam[48] and Oldenberg[49] maintained that atom-atom (N $^4S$) recombination and subsequent excited-state collisions were the main source of the high-lying electronic states.

One of the most interesting studies of the pink afterglow was that on ion concentrations reported by Brömer and Hesse.[50] Figure 2 shows the concentrations of $N_2^+$, $N_3^+$, and $N_4^+$ as a function of distance from the

8
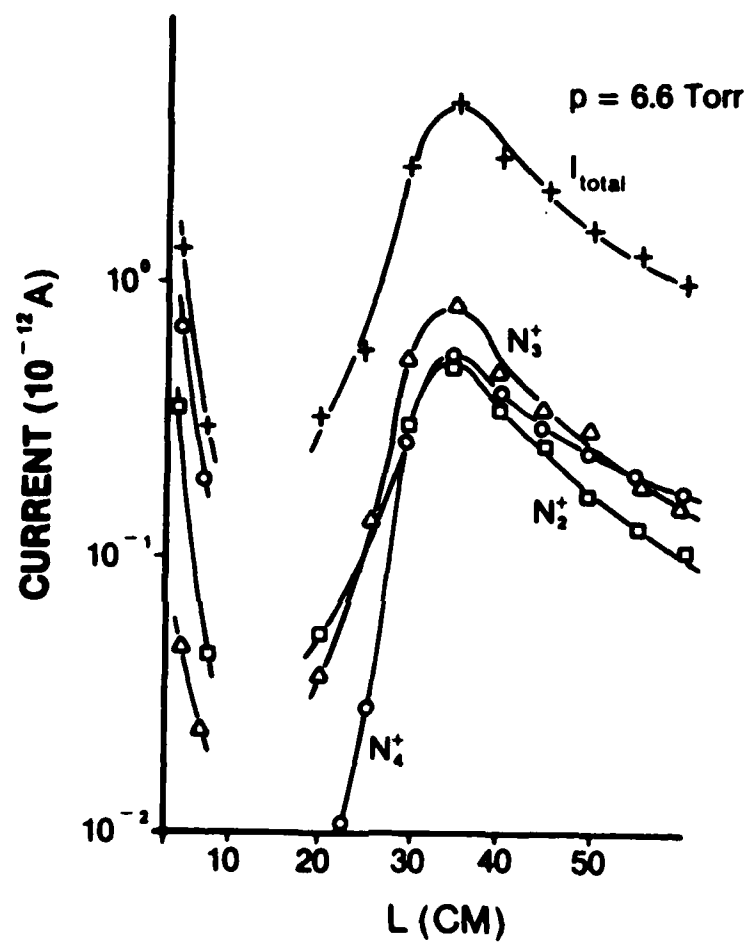
Figure 2.   Ion Wall Currents in Pink Afterglow as
            Function of Distance L (from Ref. 50).

discharge. These investigators presented plausible arguments regarding the relative populations of the various ions but were unable to identify the ionization mechanism. They did, however, present evidence that the initial ion is $N_3^+$.

Although the kinetics of the pink afterglow are not yet well defined, observations in this laboratory indicate that N-N recombination plays only a minor role, if any. This conclusion is based upon the lack of significant $1^+$ emission in the dark space preceding the afterglow, although copious amounts of $1^+$ are observed in the glow area. Tanaka's[47] measurement of only a very weak absorption by $N(^4S)$ supports this point. Also, it seems unlikely that any electronic metastable produced in the discharge could survive the many gas and wall collisions for the 5 - 15 msec time period observed in the 1-cm-diam. quartz tube.

The excited species exiting the discharge with the highest probability of survival is the vibrationally excited $N_2(X)$. For microwave-excitation conditions, kinetic modeling of Piper and Caledonia[51] has shown that v-v pumping of ground-state $N_2$ results in large amounts of high vibrational states in the 5 - 20 msec time period. However, the mechanism of energy transfer from the vibrating molecule to electronic states is still unknown. Collision-induced curve crossing, such as postulated by Campbell and Thrush[52] as a source of $N_2(a'^1\Sigma_n^-)$, is a likely process.

The mechanism of the $N_2$ dielectric-barrier discharge is understood even less than that of the pink afterglow. Relatively few studies can be found in the literature. This topic will be discussed in more detail in Section IV.

## Section III
## MICROWAVE EXCITATION

A waveguide surface-wave launcher, based on the work of Moisan, et al.,[27] was utilized as the microwave-to-plasma coupling device in the present study. Figure 3 is a schematic diagram of this "surfaguide" launcher. It was designed[53] for use at 2.45 GHz with a 12-mm-diam. plasma tube. The plasma-tube arrangement is shown in Fig. 4. The magnetron was operated at up to $\sim$ 300 W (CW), although coupling contraints typically limited the deposited power to < 200 W. The high-purity $N_2$ (99.9995% Matheson purity) was introduced into the discharge tube through a 6-mm quartz tube. The axial position of this tube was variable throughout the 12-mm discharge tube to permit introduction of the $N_2$ prior to or within the discharge as well as within the afterglow.

The high-purity $N_2$ and research-grade Ar (99.9998%) were connected through high-purity regulators and shut-off valves and Brooks Series 5850 flow-measurement and regulator valves. Although the $N_2$ metastable levels are extremely sensitive to impurity level[1]--particularly oxides of nitrogen and carbon--ultra-high-vacuum procedures were not utilized. After assembly, where Viton O-ring seals were used at glass junctions, the entire assembly was He-leak tested to ensure a minimum leak rate of $\sim 10^{-9}$ atm-cc sec$^{-1}$. Since the system was operated in an open-loop flowing arrangement, the major sources of impurities were the gas supplies and the walls of the lines, discharge tube, and afterglow tube.

Assuming that the outgassing rates of the walls are not significantly affected by the total gas pressure, published outgassing rates measured in vacuum systems can be used to estimate the wall contribution to the impurity level. The outgassing rate per unit area is measured in units of pressure times volume-flow-rate per unit area and is a weak function of time.[54] The gas flow rate is measured in pressure times volume-flow-rate units. Therefore, the impurity level (ppm) can be calculated from the outgassing rate, the gas-flow rate, and the area of the surface over which the gas must flow. From the compiled data of O'Hanlon,[54] the following relationships have been derived:

11
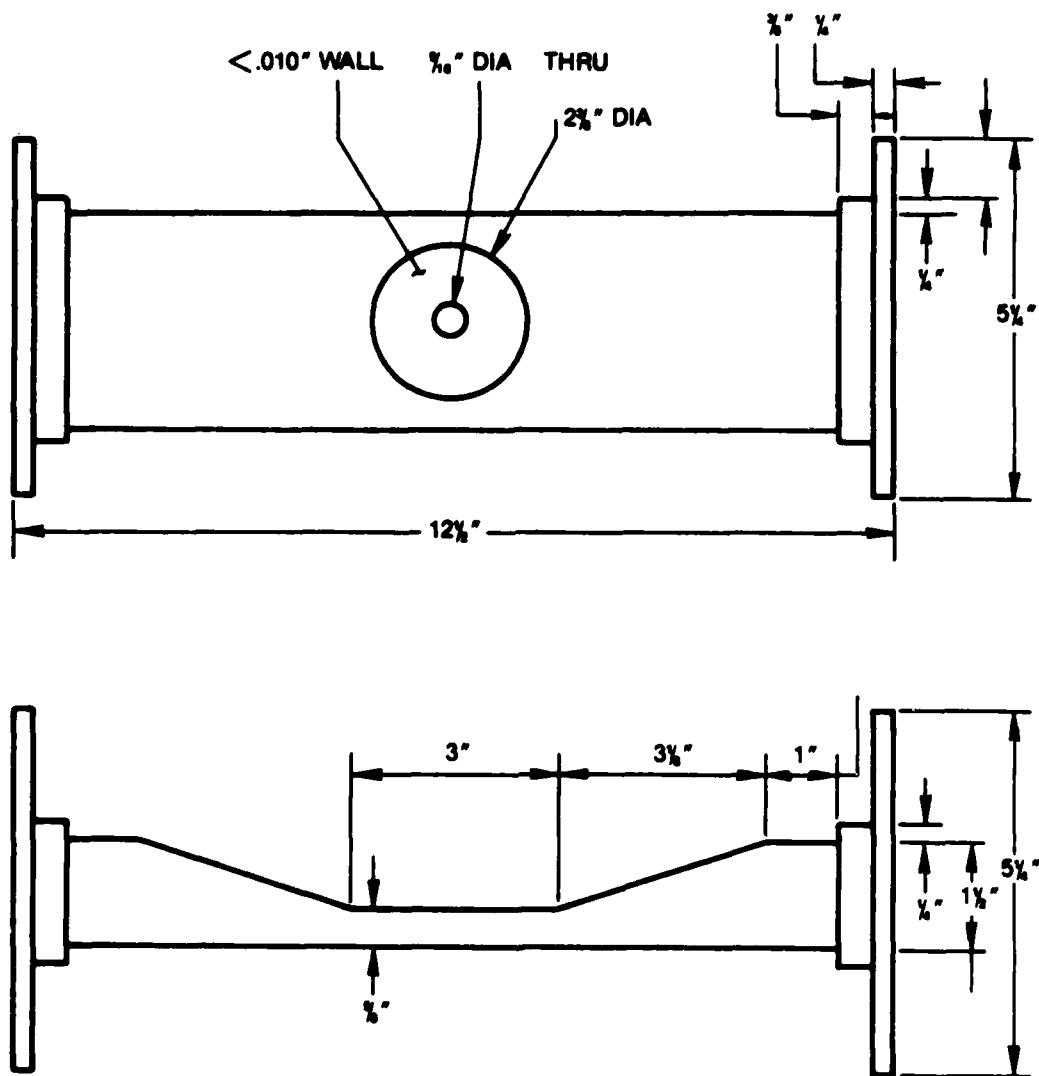
Figure 3. Schematic Diagram of Surfaguide Microwave
Surface-Wave Launcher.
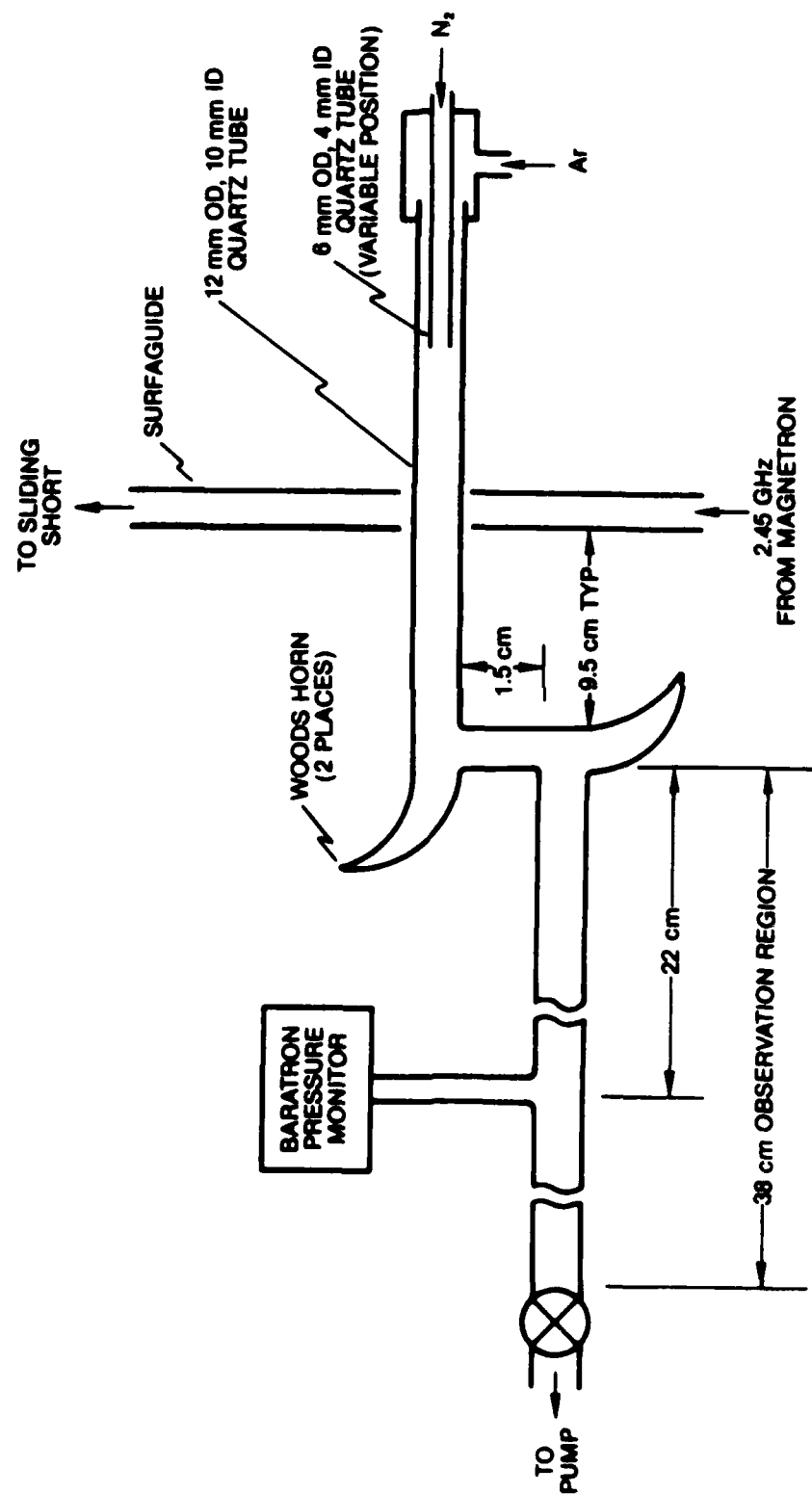
Figure 4. Schematic Diagram of Experimental Arrangement for Surface-Wave Discharge and Afterglow.

13

$$P'|_{Pyrex} = 0.58 \; \frac{A_{Pyrex}}{F_V} \; ppm \tag{1}$$

$$P'|_{OFHC \; Cu} = 3.2 \; \frac{A_{Cu}}{F_V} \; ppm \tag{2}$$

$$P'|_{Viton} = 90 \; \frac{A_{Viton}}{F_V} \; ppm \tag{3}$$

where $P'$ is the impurity level in ppm, $A$ is the exposed surface area in $cm^2$, and $F_V$ is the gas-volume flow rate in sccm. The above relationships are "worst-case;" that is, the outgassing rates are the measured values after 1 hr. of vacuum exposure without baking. The rates typically drop to one-tenth this value after $\sim$ 10 hr. For the experimental system diagrammed in Fig. 4, the gas is exposed to $\sim$ 175 $cm^2$ of quartz (considering the end point at 10 cm into the afterglow region), $\sim$ 180 $cm^2$ of OFHC copper per gas line, and $\sim$ 3 $cm^2$ total of exposed Viton O-rings. This translates to an impurity level of < 10 ppm at 100 sccm volume flow rate and < 1 ppm at the more commonly used 1000 sccm flow rate. This level is below the bottle purity. Therefore, in the absence of additional leakage during discharge operation, the purity level of the gas is dominated by the gas supply.

The surface-wave discharge has been extensively studied experimentally by Moisan and co-workers.[23-27] Two features are unique to this technique. First, the radial distribution of excited states is similar to that of the DC positive-column discharge only at very low pressures ($\leq$ 50 mTorr at 1 GHz) or at low RF frequencies; that is, as the pressure or RF frequency is increased, the density of excited states is observed to be a maximum near the walls of the discharge tube. The radial-distribution profile flattens out in the presence of an axial magnetic field or if the tube is terminated at a distance less than the plasma length, that is, if multiple wave reflections are present.

14

Secondly, the length of the discharge column is determined by the gas pressure and the RF power applied and is a strong function of the gas kinetics. Essentially, the electron density decreases with distance away from the launcher, and the discharge length is dependent upon the maintenance of sufficient electron density and electron energy to effect ionization. At low pressures ($\sim$ 50 mTorr) where electron collision frequency is small, discharge-column lengths of up to 6 m have been reported.[55] At atmospheric pressure, a plasma length of $\sim$ 18 cm has been attained, with an absorber RF energy of 200 W (915 MHz).[23]

A surface-wave discharge at high pressures differs from the low-pressure plasma in that no discharge occurs in the radial center of the tube. At < 10 Torr Ar, a relatively diffuse discharge was obtained in this laboratory in the setup shown in Fig. 4. As the pressure was increased to 20 Torr, however, the discharge consisted of "fingers" of $\sim$ 1 - 2 mm diam. which generally rotated about the inside surface of the 10-mm-ID tube. At atmospheric pressure, the fingers became fewer in number, shorter in length, and slightly smaller in diameter. The fingers were sharply defined at atmospheric pressure and more diffuse (weak glow surrounding fingers) at 20 Torr.

In contrast, the $N_2$ never formed "fingers." A somewhat diffuse glow filled the discharge tube at $\sim$ 2 Torr $N_2$ pressure. As the pressure was increased, the length decreased and the radial center became hollow. At $\sim$ 15 Torr, the discharge appeared to conform to the tube inner wall and extended no more than $\sim$ 0.5 cm from the surfaguide boundaries. A discharge in pure $N_2$ could not be maintained at pressures $\geq$ 25 Torr, even with up to $\sim$ 250 W of 2.45-GHz power.

As discussed in Section II, the atom-atom recombination mechanism of the Lewis-Rayleigh afterglow is not promising as a source of high-density molecular metastables. Therefore, observations were first concentrated on the "pink" afterglow. Figures 5 and 6 show a typical spectral scan taken in the brightest portion (visible) of a pink afterglow at 3.1 Torr of pure $N_2$. This position corresponds to $\sim$ 23 cm downstream of the discharge glow, which translates to $\sim$ 8.8 msec (plug flow). The spectral characteristics are similar to those reported by other authors; that is,

15

INTENSITY (ARB. UNITS)

$\Delta v = -1$
$v' = 4\ 1$

$0$
$4\ \ 0$

$1$
$4\ 2\ 0$

$2$
$4\ 2\ 0$

$3$
$4\ 2\ 0$

$4$
$3\ 2\ 1\ 0$

$5$
$3\ 2\ 1\ 0$

$6$
$1\ 0$

$C^3\Pi_u - B^3\Pi_g$

$\Delta v = -3$
$v' = 6\text{-}3$

$-2$
$6\text{-}2$

$-1$
$5\text{-}1$

$0$
$5\ 2\ 0$

$1$
$6\ 2\ 0$

$2$
$6\ 4\ 2\ 0$

$B^3\Pi_g - A^3\Sigma_u^+$

$\Delta v = 5$
$18\ 12\ 9$

$v' = 3\ \ 2\ \ 0$

$B^2\Sigma_u^+ - X^2\Sigma_g^+$

WAVELENGTH (nm)

300    340    380    420    460    500    540

Figure 5. Emission Spectrum of Pink Afterglow in Range 300 - 550 nm in 3.1 Torr $N_2$.
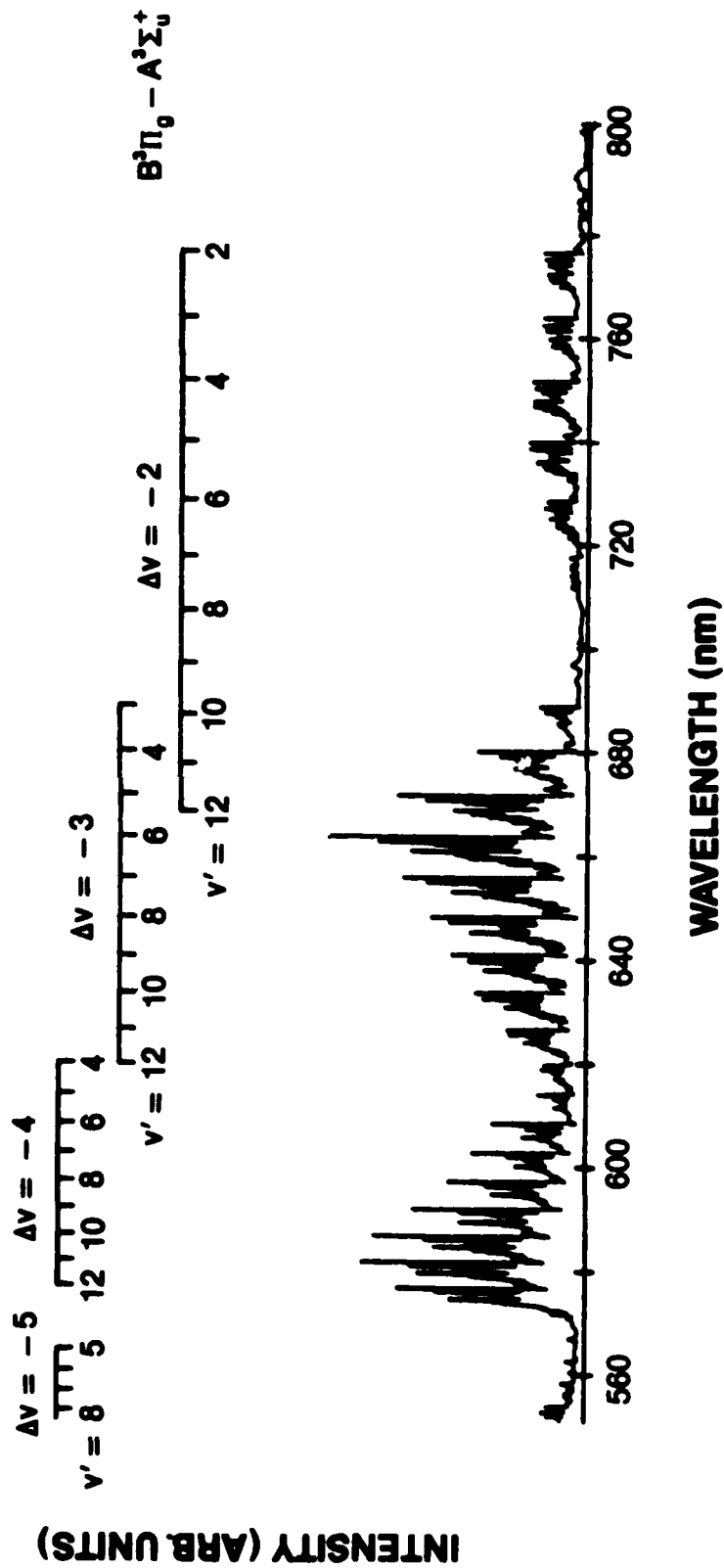
16

Figure 6. Emission Spectrum of Pink Afterglow in Range 550 - 800 nm in 3.1 Torr $N_2$.

17

the three dominant emission bands are the first- and second-positive neutral molecular bands and the first-negative ionic band. Upper vibrational levels (v') up to $\sim$ 6 are observed in the first-negative spectrum. This corresponds to an internal energy of $\sim$ 20.4 eV.

Energies of this magnitude indicate that the excited ion is formed by excitation of the $N_2^+(X^2\Sigma_g^+)$ ground-state ion by collision with an electronically excited molecule or atom. It is unlikely that any significant concentration of electronic states above 10 eV can exist for direct excitation (pooling) of two electronically excited neutral molecules for the present experimental conditions. The radiative lifetime of states above 10 eV is < 190 $\mu$sec;[2] due to numerous curve crossings, it is unlikely that high-lying vibrational levels of long-lived states exist in any significant quantity.

Energetically, selected combinations of the low-lying $N_2$ metastable states could account for the increase in molecular ions. Emission spectra measured $\sim$ 1.9 msec and 3.8 msec upstream of the position of the brightest pink afterglow emission were compared to those of Fig. 5 and 6. The 1.9-msec position corresponded to the approximate region in which the pink afterglow first became visible to the eye. The flow tube was "dark" at the 3.8-msec (upstream) position.

It should be noted here that the flow times are calculated by assuming plug flow. Because of the two right-angle bends in the apparatus, some degree of turbulence in the flow can be expected. If laminar flow exists, the actual gas-flow speed may be larger by a factor of $\leq$ 1.6.[56]

Unfortunately, it was not possible to isolate the three positions optically without affecting the glow. Therefore, it was not clear what proportion of the upstream emission spectrum was due to scatter of light originating in the bright-pink afterglow region. The vibratrional distribution of the three bands was similar at the three positions, indicating that significant scatter interference may have been present. However, the relative band intensities differed with position; that is, the ratio of peak intensities of the brightest bandhead of the first negative (v' = 0, v" = 0), the first positive (11, 7), and the second

positive (0,0) was 1:0.39:0.53 in the pink afterglow. The corresponding
ratio for 1.9 msec upstream was 1:0.28:0.17 and that for 3.8 msec
upstream was 1:0.16:0.08. Further work is needed, however, for accurate
determination of the true spectral content of the upstream positions.

An interesting characteristic of the pink-afterglow spectrum is the
presence of high vibrational levels of the first positive shown in the
$\Delta v$ = 5 sequence in the region of $\sim$ 510 - 530 nm (Fig. 5). This charac-
teristic has also been reported by Tanaka and Jursa[57] in the laboratory
auroral afterglow as well as by Ung.[22] Ung's work was later disputed by
Brennen and Shuman[58] who believed that the observation was merely scat-
tered light from the discharge. From the present observations it
appears that Ung was actually observing a pink afterglow rather than the
Lewis-Rayleigh afterglow, as he believed. The lack of measurable $N_2$(B,
v' > 12) upstream of the pink afterglow in the present measurements
shows that the discharge emission is not the source of high vibrational
levels of the first positive.

Ung[22] further observed that the first-positive intensity for v' $\leq$ 12 was
proportional to the square of the N-atom density, indicating that N-atom
recombination was the source of lower $N_2$(B) vibrational levels. In
Ung's work, however, the $N_2$(B, v' > 12) exhibited an entirely different
effect. Indications were that collisions by excited states were the
source of highly excited $N_2$(B), although Ung was unable to identify
those states.

It is unlikely that an appreciable density of any electronically excited
$N_2$ mulecule can survive the long flow from the discharge to the observa-
tion region in the present system. Using the diffusion coefficient of
133 $cm^2$ $sec^{-1}$ ($Torr^{-1}$) measured by Hays, et al.,[59] and assuming effi-
cient loss at the walls,[60] the average lifetime in the present system is
$\sim$ 1 msec. Because of the large quenching-rate coefficient[21,60] of $N_2$(A)
by N($^4$S) and the very large increase in the first-positive emission in
the pink afterglow, it is also unlikely that N-atoms leaving the dis-
charge are the souce of the pink afterglow. Additional evidence of the
absence of N($^4$S) is the low population of the high vibrational levels
relative to the lower levels in the first-positive spectrum, as shown in

19

Fig. 7. Relative populations were calculated by weighting the first-positive emission intensities with measured[2] transition probabilities.

Vibrationally excited ground-state molecules are the most likely precursors of the electronically excited states. Calculations of Piper and Caledonia[51] have shown up to $\sim 0.01\%$ of the ground-state molecules to be in $v > 20$ in a 1-Torr microwave-initiated afterglow after $\sim 5$ msec of v-v pumping. As the density of $N_2(X, v \geq 25)$ increases, a collision-induced spin change could result in

$$N_2(X, v \geq 25) + M \rightarrow N_2(A) + M \qquad (4)$$
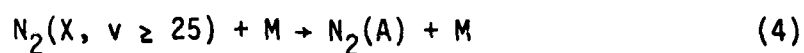
where M is a nitrogen molecule or atom. The mechanism of production of $N_2^+$ ions from $N_2(A)$ and $N_2(X, v)$ is poorly understood, but N-atoms seem to be a byproduct of this process. As the N-atom density increases, the speed of (4) will increase since the curve-crossing process is more efficient for the case where an atom is the collision partner.[33] However, collisional quenching of $N_2(A)$ by $N(^4S)$ will also increase, limiting the maximum attainable $N_2(A)$ density.

Attempts in this laboratory to observe known effects of $N_2(A)$, such as observation of Vegard-Kaplan bands and laser-induced fluorescence, in the pink afterglow have failed. If one assumes that the population of the $N_2(A)$ precursor is $< 0.01\%$ of the $N_2$ density, then a conversion efficiency of 10% would result in an $N_2(A)$ density of only $\sim 10^{13}$ cm$^{-3}$. An increase in $N_2$ density is required in order to reach higher $N_2(A)$ densities. However, as the total pressure is increased, the pink afterglow is formed further upstream (closer to the discharge). The maximum pressure at which the pink afterglow could be produced with $\sim 150$ W of 2.45-GHz microwave input was 15 - 18 Torr. Above this pressure, only the Lewis-Rayleigh afterglow (first-positive bands) could be observed.

Although it was not possible to maintain a discharge in pure $N_2$ at pressures above $\sim 20 - 25$ Torr in the present apparatus, an atmospheric-pressure discharge in Ar could easily be obtained. Energy transfer
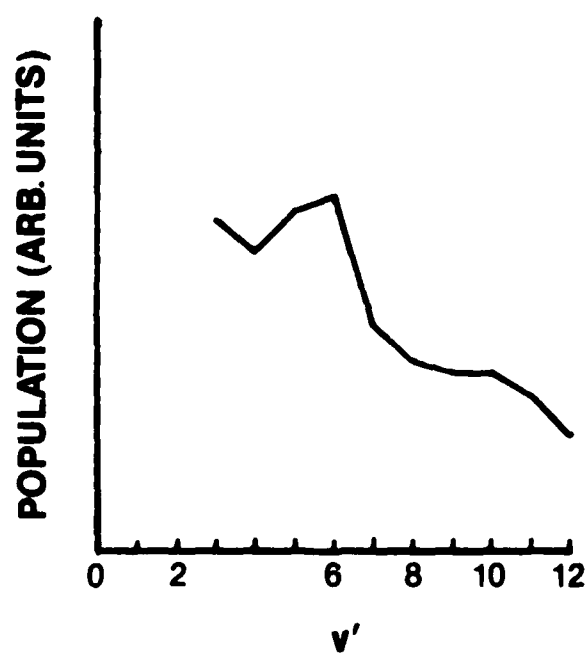
Figure 7. Plot of Relative Population of Vibrational Levels of $N_2(B^3\pi_g)$ in Pink Afterglow (from Emission Spectrum of Fig. 6).

21

between the Ar $^3P_0$ and $^3P_2$ metastables and $N_2(X)$ results in an $N_2(C)$ or $N_2(B)$ state molecule; the reported rate constants exceed $10^{-11}$ $cm^3$ $sec^{-1}$.[61,62] The application of this reaction is a common technique for excited-state studies since $N_2$ electronic states can be created in a low-pressure flowing stream of $N_2$ without also creating N-atoms. However, at higher pressures, collisional mixing of the $Ar(^3P_0, \, ^3P_2)$ with radiative $Ar(^3P_1, \, ^1P_1)$ levels reduces the effective metastable lifetime.[28] Even more damaging to the lifetime, however, is the three-body reaction

$$Ar^* + 2Ar \rightarrow Ar_2^* + Ar \qquad (5)$$

The rate coefficient for this reaction is reportedly[63] $= 10^{-32}$ $cm^6$ $sec^{-1}$. The maximum collisional lifetime at 300-Torr Ar would, thus, be $\simeq 1$ μsec. Therefore, mixing $N_2$ downstream of an Ar discharge is practical only at low pressures.

Operating the discharge in a mixture of Ar and $N_2$ at high pressures is possible only with relatively small quantities of $N_2$. However, mixing of flowing $N_2$ inside an Ar discharge resulted in the attainment of $N_2$ partial pressures up to ∿ 200 Torr. This mixing was effected by inserting the $N_2$ flow tube of Fig. 4 into the high-pressure Ar "finger" discharge, as described earlier in this section. With the exit position of the $N_2$ flow tube corresponding to the downstream edge of the surfaguide, the discharge changed from a blue Ar finger discharge upstream of the $N_2$ flow-tube exit to a yellow-orange $N_2$ discharge downstream.

The afterglow spectrum resulting from this arrangement shows almost exclusively the first-positive bands of a Lewis-Rayleigh afterglow. Only CN emission, a common impurity in $N_2$ discharges,[64] appears to be present at wavelengths below 500 nm. Figure 8 shows a representative $N_2$ B → A spectrum recorded in the afterglow of a 289-Torr Ar, 11-Torr $N_2$ microwave discharge. Figure 9 shows the B-state relative v' populations resulting from the measured emission. Since the distribution is indicative of N-atom recombination and no indication of other electronically
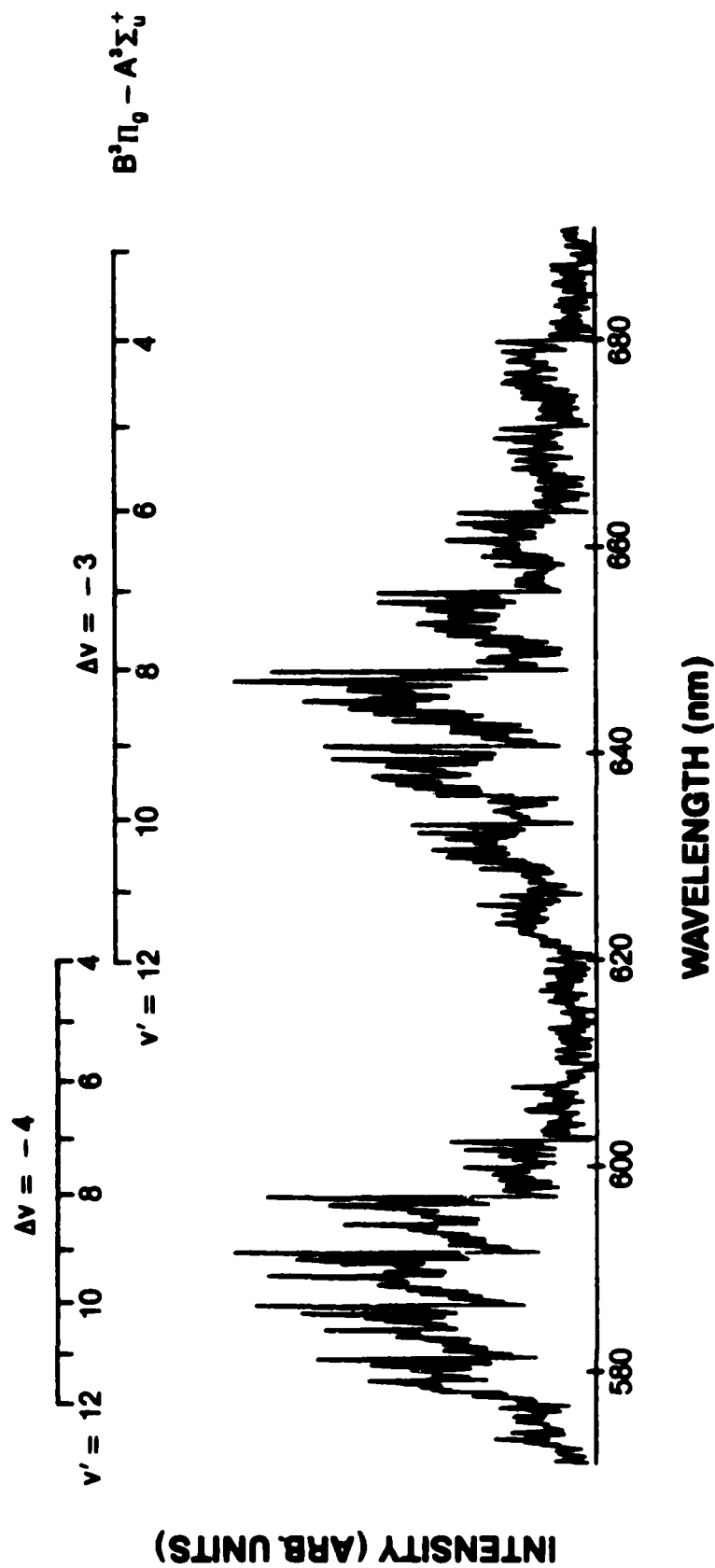
Figure 8. First-Positive Emission Spectrum of Afterglow of 289-Torr Ar + 11-Torr $N_2$ Microwave Discharge.

23
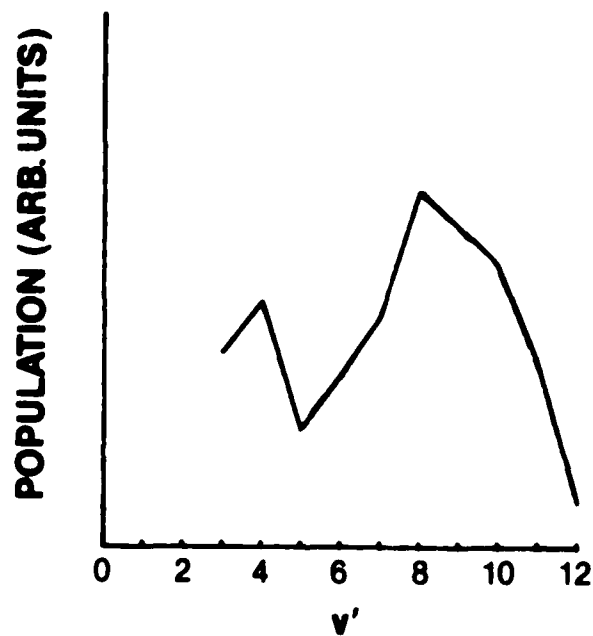
Figure 9.   Plot of Relative Populations of
            Vibrational Levels of $N_2(B^3\pi_g)$
            in Ar + $N_2$ Afterglow (from
            Emission Spectrum of Fig. 8).

excited $N_2$ states is present, it appears that the only long-lived species produced by this discharge technique is the N-atom.

In summary, the low-operating-pressure regime of the "pink afterglow" appears to limit the maximum excited-state density. At $N_2$ pressures $\geq$ 10 Torr, N-atom populations will restrict the maximum excited-state densities. The microwave excitation technique does not seem to be amenable to production of large excited-state densities.

## Section IV
## DIELECTRIC-BARRIER EXCITATION

The first report of a nitrogen emission spectrum in a dielectric-barrier discharge was made in 1939,[65] although the coaxial glass configuration employed had been previously used for the generation of ozone.[66] At that time the discharge was assumed to be composed of a myriad of discharges, each having a very small cross-sectional area. The novel spectrum seen by the first investigators consisted primarily of second-positive and Vegard-Kaplan bands of $N_2$ and $\gamma$-bands of NO. Since that time the dielectric-barrier configuration--also referred to as an "ozonizer" or a "silent discharge"--has been used to produce spectra which are relatively free of the ordinarily strong first-positive spectra.[1,2]

This discharge configuration is unique in that it can operate at high pressures (in excess of 1 atm), does not require gas contact with metal electrodes, and does not heat the gas appreciably.[65] However, until the introduction of metastable transfer emission spectroscopy (MTES)[67] less than ten years ago, little interest was shown in the dielectric-barrier discharge as a source of metastable A-state nitrogen. The earlier lack of interest appears to be due primarily to the lack of high-pressure applications. Most spectroscopic studies on $N_2$ have been performed at low pressures in order to minimize collision effects; an atmospheric-pressure source for MTES, however, would make that technique much more useful.

Recently, large metastable concentrations from a dielectric-barrier discharge have been reported for pressures of $\leq$ 20 Torr[14,68] and for atmospheric pressure.[17,69] These reports are particularly significant to the present effort because of the involvement of metastable energy transfer. The initial report of low-pressure studies[68] claimed $N_2(A)$ densities of > $10^{16}$ $cm^{-3}$, but later it was conceded that the discharge may extend into the "afterglow" area.[14] The high-pressure studies[17,69] do not specify an $N_2(A)$ density but report achievement of a linear MTES response for sample densities corresponding to $\sim 10^{13}$ $cm^{-3}$.

Unfortunately, these reports contain the erroneous conclusion that the majority of the metastable transfer of energy occurs in the afterglow. The low-pressure work[14,68] is particularly misleading. The presence of second-positive bands more than 100 msec downstream of the discharge region which exhibit little change in intensity with distance (time) is a sign of continuous electronic excitation. In this study much of the "afterglow" region was covered with a grounded conductor,[68] and an obvious current path was detected when a grounded filament was placed in the observation region, even when a glass-wool plug was inserted between the discharge region and the downstream observation region.[14] Furthermore, the flow rate at a pressure of 1 - 5 Torr was only 2 - 5 sccm, much too low to prevent electronically excited species from destruction at the walls.

Although the presumption of an afterglow appears to be incorrect and the discussions of the discharge mechanism and spectral characteristics can stand improvement, this work demonstrates some useful characteristics of the dielectric-barrier discharge: (1) at low pressure it was relatively easy to achieve an extended discharge, well beyond the dielectric-covered electrodes; (2) when the dielectric was removed from one of the electrodes, the discharge appeared to exist only within several millimeters of that electrode;[68] (3) low first-positive band intensities were observed relative to the second positive.

The collisional transfer of energy reported in the high-pressure MTES studies[17,69] also appears to occur in a discharge region. The trace materials were added into the flowing-gas coaxial-electrode configuration through a small dielectric tube which terminated only ∿ 5 mm from the dielectric covering of the center electrode. It is quite probable that electric-field leakage into this region results in some direct electronic excitation of $N_2$ and/or the trace species being admitted.

The most thorough analysis of the afterglow of a dielectric-barrier $N_2$ discharge was performed by Noxon.[16] His apparatus was configured in a flowing closed-cycle loop; the discharge was coaxial, having a 3-mm gap, and the observation region began ≳ 0.5 sec after the gas exited the discharge region. Emission measurements made at pressures ranging from

27

20 to 760 Torr are consistent with reasonable afterglow kinetics. Both the first-positive and the Vegard-Kaplan bands were weak but measurable using long path lengths or long integrating times. Weak $N(^2P)$ emission was also observed. Impurity emissions of NO ($\gamma$ and $\beta$ bands), NH, CN, and atomic O (297.2 and 557.7 nm) were observed at varying levels, depending principally upon the source of $N_2$ and the level of scrubbing.

Noxon's careful analysis[16] was based upon the accepted kinetic rates existing at that time (1961). His calculations show an $N(^4S)$ density of $8 \times 10^{10}$ cm$^{-3}$ existing $\sim 0.5$ sec into the afterglow and a Vegard-Kaplan emission which, using a presently accepted radiative lifetime of $\sim 2$ sec,[2] corresponds to an A-state density of $\sim 10^{12}$ cm$^{-3}$. Assuming that three-body atom-atom recombination is the dominant loss process for $N(^4S)$, Noxon's ground-state N-atom density extrapolates to $\sim 8.1 \times 10^{10}$ cm$^{-3}$ at the discharge exit (using a rate coefficient of $10^{-32}$ cm$^6$ sec$^{-1}$, an approximation from Refs. 19 and 70).

Several errors, however, exist in Noxon's analysis, the most serious being failure to account properly for collisional deactivation of $N_2(B)$. From an extrapolation of low-pressure data, he assumed that his measurement of first positive ($1^+$) resulted from the emission of one photon for every forty $N(^4S)$ atom-atom recombination events, independent of pressure.

More recent reports,[7,34,36-38,71-73] however, have shown the existence of strong collisional coupling among the $N_2(B)$, $N_2(W)$, $N_2(B')$, $N_2(A)$, $N_2(a)$, $N_2(a')$, and possibly even the $N_2(X)$ states at selected vibrational levels. The coupling ability is explained by the close proximity of the inter-nuclear turning points of these states. The vibrational-level selectivity is a result of the energy resonance of the neighboring electronic-vibrational states. For example, the compiled data of Lofthus and Krupenie[2] show that the $N_2(B, v = 6)$ lies only 21 cm$^{-1}$ ($2.6 \times 10^{-3}$ eV) below the $N_2(W, v = 7)$. A rate coefficient of $1.3 \times 10^{-10}$ cm$^3$ sec$^{-1}$ has been measured by Benesch[36] for this, indicating that an equilibrium density of $W \gtrsim B$ will result, even at relatively low pressures.

The exchange process of W $\rightleftarrows$ B becomes even more interesting with the realization that another close resonance occurs at $N_2(B, v = 12) \rightleftarrows N_2(W, v = 14)$. The transfer from B $\rightarrow$ W is exothermic by 32 $cm^{-1}$ (4 x $10^{-3}$ eV). In addition, a two-quanta vibrational relaxation of $N_2(W, v = 14 \rightarrow 12)$ would be exothermic to one quantum jump of $N_2(X, v = 1 \leftarrow 0)$ by 47 $cm^{-1}$ (5.8 x $10^{-3}$ eV). One would expect this rate to be very fast at atmospheric pressure because of the large background of $N_2(X, v = 0)$. The energy match of $N_2(W, v = 9 - 12)$ with $N_2(B)$ levels is poor, and the radiative lifetime of $N_2(W)$ is estimated to be < 100 $\mu sec$ for $v' > 4$.[2] It appears, therefore, that atom-atom recombinations entering the $N_2(B, v = 12)$ state would not all be seen radiatively in the high $v'$ of the first-positive spectrum since these molecules would be trapped rapidly in the $N_2(W)$ state and radiatively decay in the infrared to lower $v'$ values of $N_2(B)$. This may explain the appearance of the $v' = 6$ first-positive emission recorded by Noxon, although his resolution was not sufficient to permit conclusions concerning the $v'$ distribution.

Unfortunately, a more-thorough analysis is needed in order to determine all of the energy matches appearing in the vicinity of the $N_2(B)$. In the absence of more-accurate quantitative data, a B-state collisional-loss rate coefficient of 2 x $10^{-12}$ $cm^3$ $sec^{-1}$ was applied to Noxon's data. The result was an increase in his calculated $N(^4S)$ density by a factor of $\sim$ 2 at 74 Torr and by a factor of $\sim$ 7 at 760 Torr. A correction to his listed $N(^2P)$ density was also made, based upon a 12-sec radiative lifetime rather than the $\sim$ 180 sec specified in his text. This yielded more reasonable values for the ratio of $N(^2P)/N(^4S)$ of $\sim$ 1% at most pressures. Using the correction factor the maximum $N(^4S)$ atom density of $\sim$ 3 x $10^{12}$ $cm^{-3}$ appears at 74 Torr. If the large rate coefficient of Benesch[36] is applied, this density increases to $\sim$ 2 x $10^{13}$ $cm^{-3}$. With these two values as the lower and upper bounds, the atom density exiting the discharge extrapolates to 0.32 - 3.2 x $10^{13}$ $cm^{-3}$ at 74 Torr and 0.06 - 3.7 x $10^{13}$ $cm^{-3}$ at 760 Torr.

Over most of the pressure range, then, Noxon appeared to have $\sim$ $10^{12}$ - $10^{13}$ $cm^{-3}$ $N(^4S)$ atom density at the discharge exit. At $10^{12}$ $cm^{-3}$ density the quenching rate of discharge-produced $N_2(A)$ by $N(^4S)$ would be approximately exponential with a 20-msec time constant, assuming

$[N_2(A)] >> [N(^4S)]$, [ ] denoting number density. This means that one-
half of the $N_2(A)$ states are quenched within the first $\sim$ 15 msec after
exiting the active discharge region. At the higher atom density of
$10^{13}$, only $\sim$ 0.1% of the discharge-produced $N_2(A)$ would still exist
15 msec into the afterglow region. If the atom density can be limited
to $\leq 10^{12}$ $cm^{-3}$, then quenching of metastables by $N(^4S)$ can be tolerated.

As mentioned previously, the density of the $N_2(A)$ state observed by
Noxon was $\sim 10^{12}$ $cm^{-3}$. This is calculated using the currently accepted
radiative lifetime[2] of 2 sec and assuming $[N(^4S)] = 10^{12}$. That is, only
one photon will be seen for every $\sim$ 100 molecules existing. If the atom
density had been significantly higher than $10^{12}$, the $N_2(A)$ might have
been several orders of magnitude higher at the discharge exit.

It should be noted here that Caledonia, et al.,[41] present an alternative
mechanism as the source of the first positive observed by Noxon. They
show that the observed B $\rightarrow$ A emission at high pressures can be explained
by the pooling of two $N_2(A)$ molecules, although this argument does not
agree with the limited lower-pressure data.

The mechanism of excitation within a dielectric-barrier discharge is not
well understood. As mentioned previously, the original paper by Wulf
and Melvin[65] described the discharge as being composed of many dis-
charges having small cross-sectional areas. Several recent reports on
discharges between dielectrics[74] and on ozonizer discharges[11,12,75] have
confirmed this observation using pure $O_2$ or air. Bagirov[74] observed
that as the gas pressure decreased, the number of microdischarges
increased--but the energy of each microdischarge decreased. Hirth,
et al.,[12] measured some of the characteristics of the individual micro-
discharges and found the diameter to be $\sim$ 0.1 mm, the time duration to
be a few nanoseconds, the current density to be a few kiloamperes per
square centimeter, and the gas temperature to be high. Kogelschatz[11]
reported $\sim$ 0.1 - 1 nC of charge transferred in each microdischarge, with
the value increasing with an increase in pressure or gap spacing. He
also reported an electron density of $10^{14}$ - $10^{15}$ $cm^{-3}$ and the value of
the electric field in the gap to be near the critical value where ioni-
zation is approximately equal to attachment.

30

The report of Heuser and Pietsch[75] on the spatial distribution of ozone is interesting. For a fast pulse the concentration of $O_3$ was fairly uniform along and across the gap. For a slowly varying sine-wave excitation, however, the ozone concentration was greater near the electrode/ dielectric surfaces and was at a maximum at the dielectric-covered anode. This indicates the possibility of anode space charge (electrons) playing a role in $O_2 + O$ recombination. If this effect also exists in the $N_2$ dielectric-barrier discharge, the low number density (relative to RF and conduction discharges) of $N(^4S)$ atoms may be explained by a rapid recombination within the discharge region. This, in turn, may represent a fast source of $N_2(A)$. Unfortunately, the space charge may also serve as an efficient quencher of molecular or atomic metastables through collisions of the second kind.

The preceding discussion points out the difficulties in using existing data and theories to determine the suitability of the dielectric-barrier configuration as a source of metastable $N_2$ in usable quantities ($\geq 10^{14}$ $cm^{-3}$). Consequently, the coaxial dielectric-barrier discharge tubes shown schematically in Figs. 10 and 11 were constructed. The arrangement of Fig. 10 was used for radial measurements of discharge and afterglow spectra, while the apparatus of Fig. 11 allowed for long-path-length axial observation of the afterglow.

The outer electrode was connected to ground potential; and a bipolar, approximately sinusoidal electrical waveform was applied to the inner cylindrical conductor. The electrical circuit is described in Section VI; the voltage was variable from 0 to ± 12 kV (peak), and the normal operating frequency range was 5.5 - 7.5 kHz. The discharge gap was selectable in the range 1 - 3 mm by appropriate selection of the inner glass tubing.

Bottled $N_2$ (Matheson purity, 5 ppm maximum impurity) and Ar (Airco Grade 5.8) were mixed upstream and passed through a purifier before entering the discharge tube. The active material of the purifier, T-resin,[76] has been reported to reduce oxygen impurities from an initial 100 ppm to < 50 ppb.[77] After leaving the filter, the gas passes over $\sim$ 90 $cm^2$ of OFHC tubing, $\sim$ 320 $cm^2$ of quartz or Pyrex tubing, and < 1 $cm^2$ of exposed
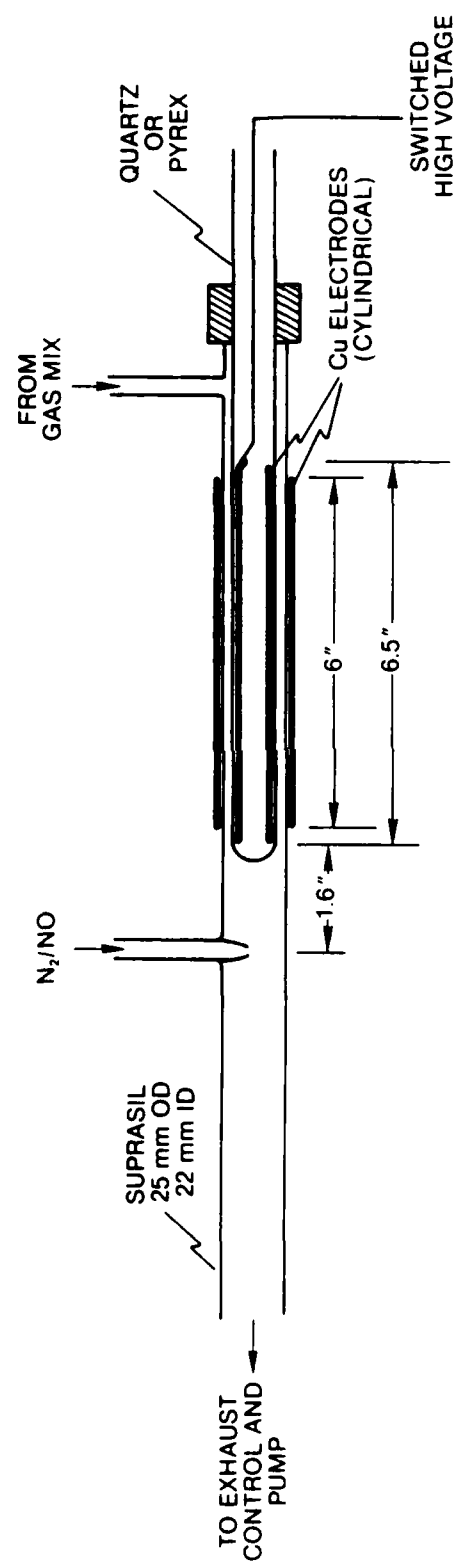
31

Figure 10. Schematic Diagram of Straight-Flow Configuration of Coaxial Dielectric-Barrier Discharge and Afterglow Tube.
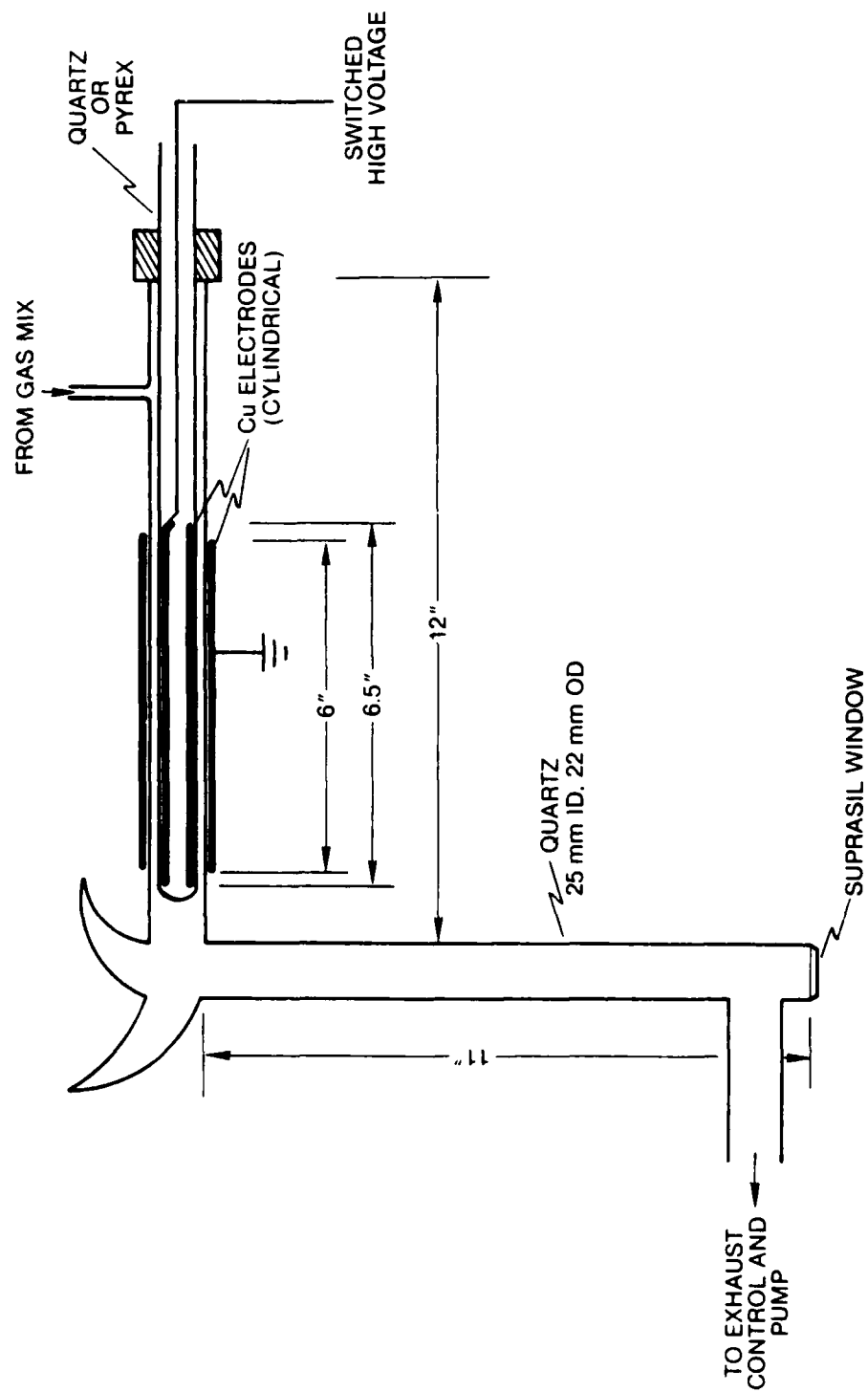
32

Figure 11. Schematic Diagram of Coaxial Dielectric-Barrier Discharge and Afterglow Tube for Axial Afterglow Observations.

33

Viton O-rings. From the arguments presented in Section III, the maximum impurity level due to wall outgassing would be ~ 0.6 ppm at 1000 sccm volume flow rate upon first sealing the system; this rate would then drop to ~ 60 ppb after ~ 10 hr of opertion, assuming that vacuum outgassing rates apply. In contrast to the microwave experimental setup, the gas purity of the dielectric-barrier configuration is limited by the outgassing of the walls, but the total purity is improved over the microwave setup by at least one order of magnitude.

Figure 12 shows typical voltage and average-current waveforms for the setup of Fig. 10. The current waveform represents an average of 256 traces of the total discharge current. A single-shot current waveform is shown in Fig. 13 and is consistent with previous observations discussed above that the discharge is not diffuse but is actually composed of many small discharges.

The macroscopic operation of the discharge is illustrated by the waveforms of Fig. 12. The 337.1-nm emission is, in general, proportional to the discharge current. The current waveform has two components, 1) displacement current due to charging of the dielectric, and 2) discharge current. The total current as well as the emission is zero at the peak of the voltage waveform. No significant current is flowing at this point. As the voltage changes, however, displacement current flows in the two dielectrics as well as in the gap.

Figure 14 shows an equivalent simplified circuit. During continuous operation, the discharge extinguishes whenever the glass dielectrics have charged sufficiently that the gap voltage becomes small. As the switch of Fig. 14 reverses the polarity across the series capacitors (discharge tube), the majority of the voltage drop is seen on the gap since $C_G$ is small compared to the capacitance of the dielectrics. As the gap voltage becomes sufficiently large to effect a breakdown, the gap takes on the characteristics of a variable resistor [$R_G$ of Fig. 14(b)], with the voltage drop being determined by the overall tube voltage less the drop across the charging dielectrics.

34
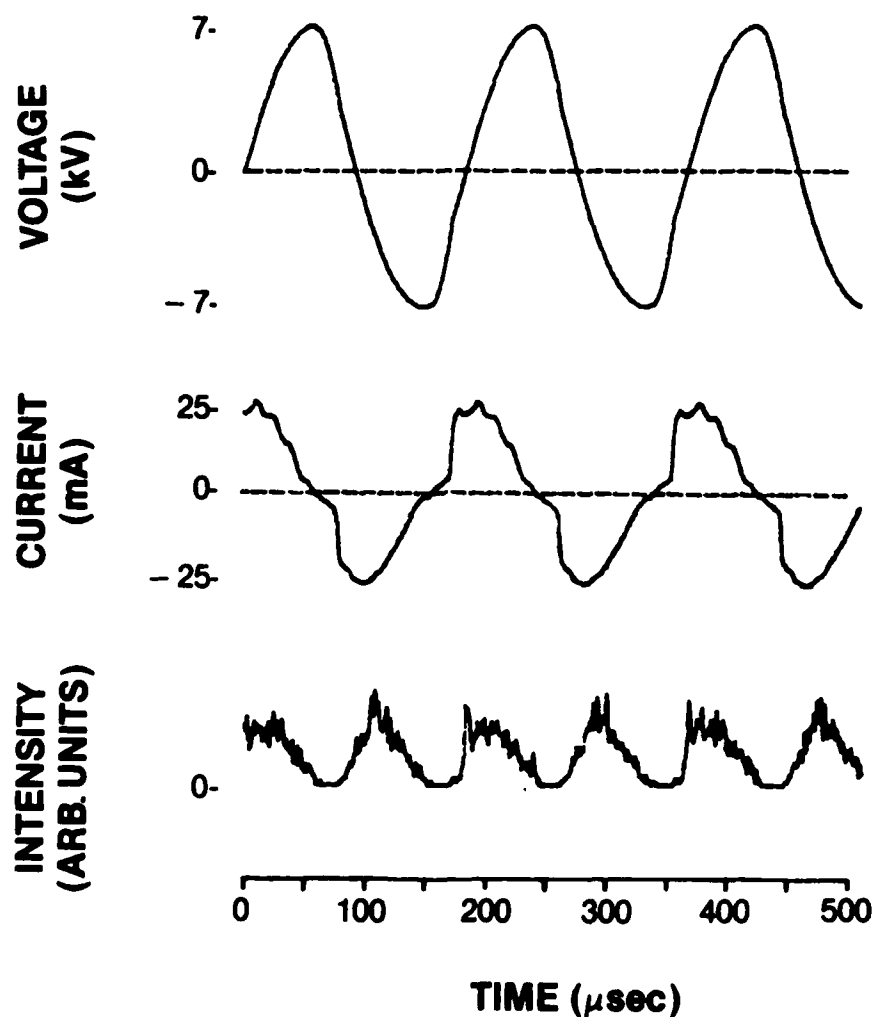
Figure 12.  Voltage, Average Current, and Intensity
(337.1 nm) Waveforms of Typical $N_2$
Dielectric-Barrier Discharge (200-Torr
$N_2$ Pressure, 3-mm Gap Spacing, 1.5-mm
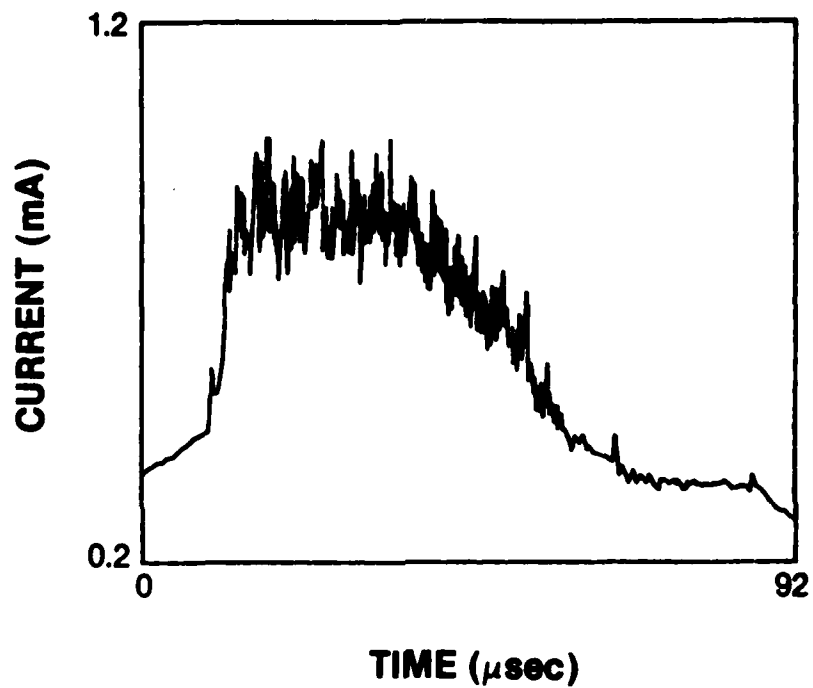Quartz Outer Dielectric, 1.25-mm Pyrex
Inner Dielectric).

Figure 13.  Half-Cycle Current Waveform (Single
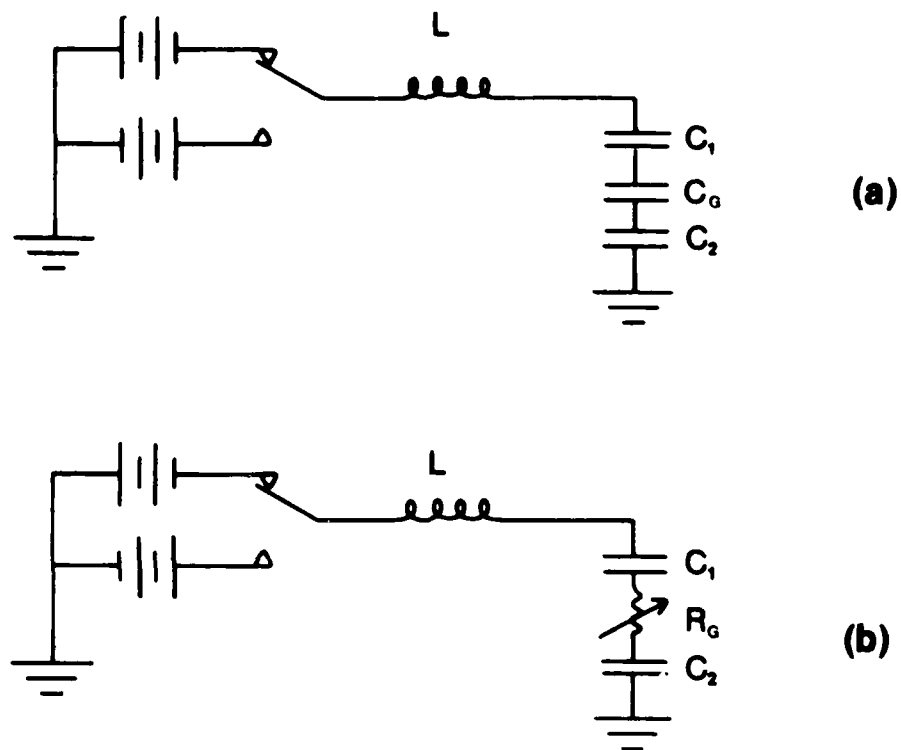Shot) of Typical $N_2$ Dielectric-Barrier
Discharge.

Figure 14. Electrical Schematic of Dielectric-Barrier-
Discharge Simplified Equivalent Circuit for
(a) No Discharge and (b) Discharge.

The current flow in the circuit is a function of the gap voltage and discharge kinetics and cannot be modeled easily. This limits the ability to calculate a self-consistent gap voltage. However, if one assumes that the gap voltage is approximately zero at the peaks of the measured waveform, then the time integral of the measured current waveform can be scaled to the voltage waveform and an equivalent gap voltage, and thus E/N, can be calculated.

Figure 15 shows the result of this calculation applied to the waveforms of Fig. 12 for the 50 - 150 μsec interval. Discharge initiation occurs with ∿ 3600 V on the 3-mm gap. For the 200-Torr pressure within the gap, the initial breakdown field corresponds to E/N = 180 Td. Unlike volume discharges, however, a high E/N is maintained for a significant period of time. As a localized arc is formed within the gap, the localized E/N falls, extinguishing the arc, followed by an increase in localized E/N. The end result is the deposition of power into the gas at a much higher E/N than possible in a discharge gap having no dielectric ballast.

The emission spectra of the dielectric-barrier discharge reveals several interesting characteristics. First, the first-positive spectrum in pure $N_2$ shows little emission from the high vibrational levels. Instead, as shown in Fig. 16, the 575 - 615 nm region consists primarily of the Gaydon-Herman green system ($H^3\phi_u - G^3\Delta_g$). This is the region in which the transition probabilities for the first-positive bands are greatest for the commonly observed v' = 9 - 12.

In the 620 - 690 nm region, however, emission from the lower vibrational levels of the first positive is observed. Figure 17 shows the relative $N_2(B)$ vibrational population indicated by the emission intensities of Fig. 16. The presence of low v' in the absence of high v' of the first-positive system indicates that $N(^4S)$ atom-atom recombination plays only a minor role, if any, in formation of the $N_2(B)$. Direct electronic excitation and $N_2(C)$ radiative transitions are the most likely B-state populating mechanisms.

Secondly, the emission spectrum shows the presence of several highly excited electronic states--the Herman infrared (exact upper level
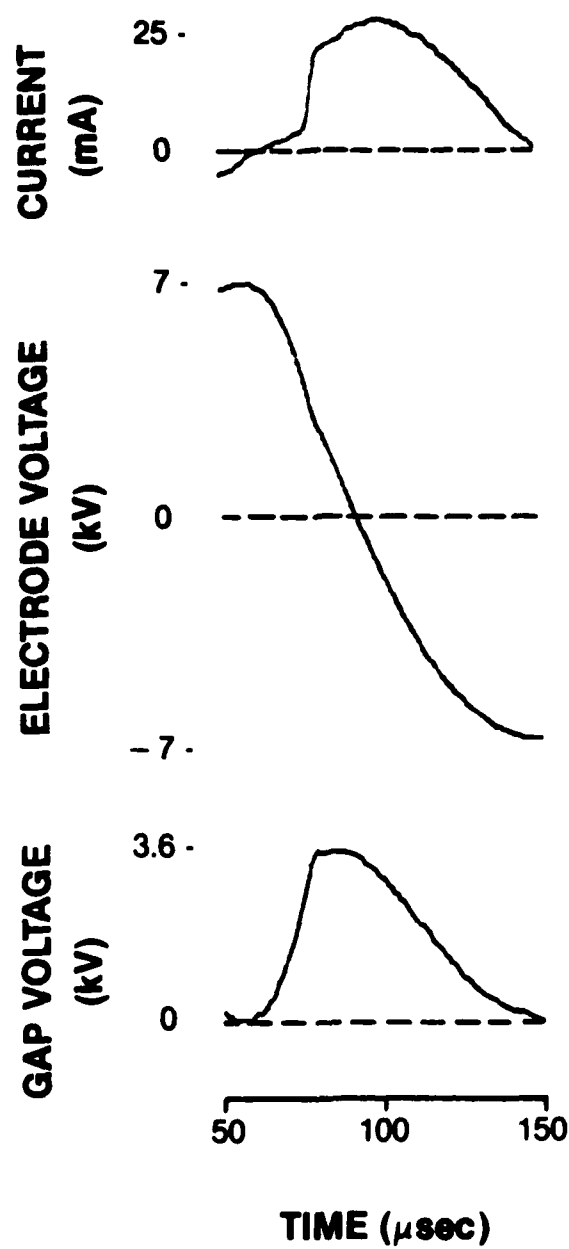
Figure 15.  Measured Current and Electrode-
Voltage Waveforms and Calculated
Gap-Voltage Waveform of an $N_2$
Dielectric-Barrier Discharge
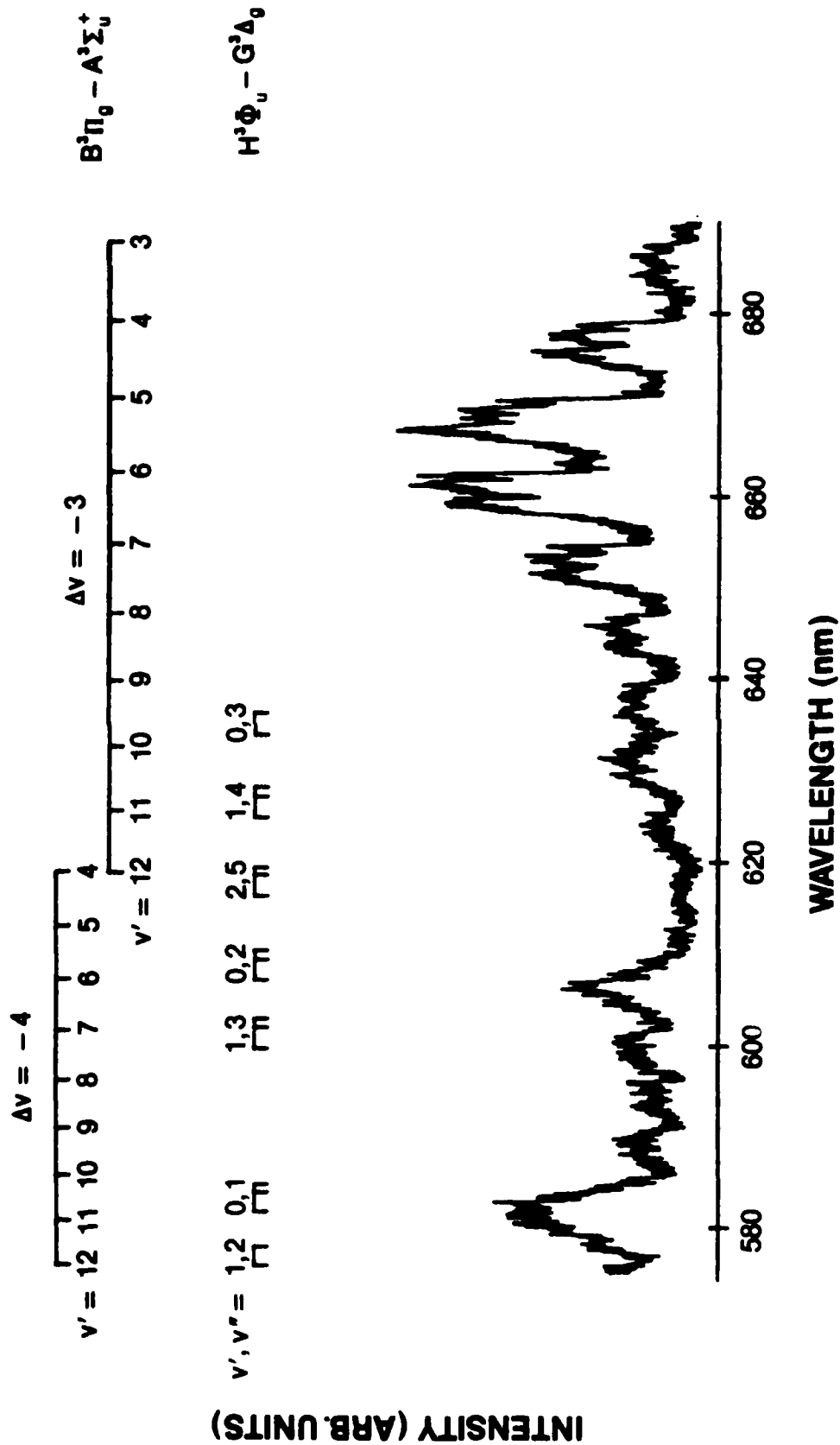(Same Conditions as Fig. 12).

39

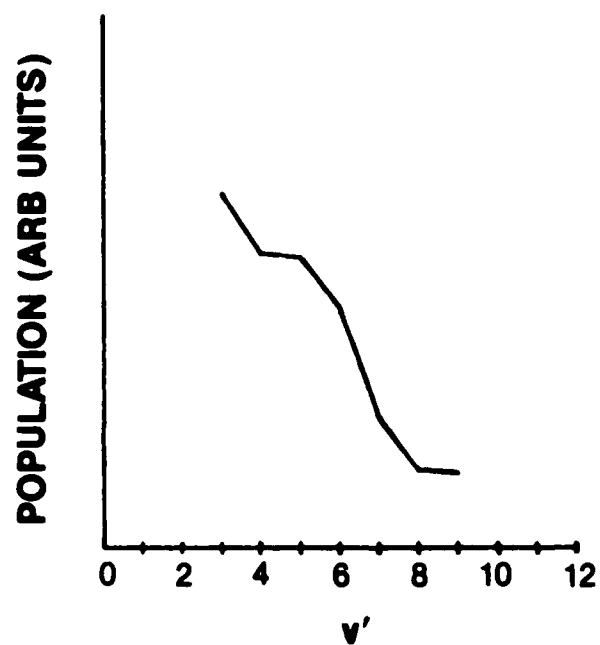Figure 16. Emission Spectrum in 575 - 690 nm Range of Typical N₂ Dielectric-Barrier Discharge.

40

Figure 17.  Plot of Relative Populations
of Vibrational Levels of
$N_2(B^3\pi_g)$ in $N_2$ Dielectric-
Barrier Discharge (from Emis-
sion Spectrum of Fig. 16).

41

unknown but suspected to lie near the $H^3\phi_u$), the Gaydon-Herman green system with the $H^3\phi_u$, $v = 0$ lying at $\sim 13.1$ eV, and the second positive with the $C^3\pi_u$, $v = 0$ at $\sim 11.1$ eV. Figure 18 shows the Herman infrared spectrum; the second-positive spectrum is displayed in Fig. 19. By far, the most intense emission is within the second positive. The intensity scale of Fig. 19 is more than two orders of magnitude larger than the scales of Figs. 16 and 18.

A third interesting feature of the dielectric-barrier-discharge spectrum is the very small amount of first-negative $N_2^+$ emission compared to second positive. Although $N_2^+(B, v' = 0 - 2)$ are measured, the most intense line $v' = 0$, $v'' = 0$ at 391.4 nm is only $\sim 0.3\%$ of the 337.1-nm $v' = 0$, $v'' = 0$ second positive.

The spectra discussed above were taken near the downstream end of the discharge tube. As shown in Fig. 10, the inner electrode extends $\sim 0.25$ in. beyond the outer electrode. The above spectra were recorded in the center of this open region. By positioning the spectrometer field of view near the downstream edge of the inner electrode, the effect of electrode polarity can be observed. Figure 20 shows the relationship in time between the second-positive 337.1-nm emission and the 391.4-nm first negative. The half-cycle at which the 391.4-nm emission is minimal corresponds to the half-cycle during which the inner electrode (maximum field of view) is the anode. This is reasonable since the $N_2^+$ ions would not be expected to survive for a long period of time in the area of maximum electron density.

Figures 21 and 22 show the temporal relationship of emission recorded in the center of the extended region and near the edge of the outer electrode, respectively. It is interesting to note that the 662.4-nm emission ($v' = 6$, $v'' = 3$) of the first-positive system follows the second-positive system in timing, indicating either a similar excitation mechanism or radiative coupling.

From the discharge observations discussed above, it appears that the mechanism for population of the $N_2$ triplet manifold in a pure $N_2$ dielectric-barrier discharge is via electronic excitation and cascading.
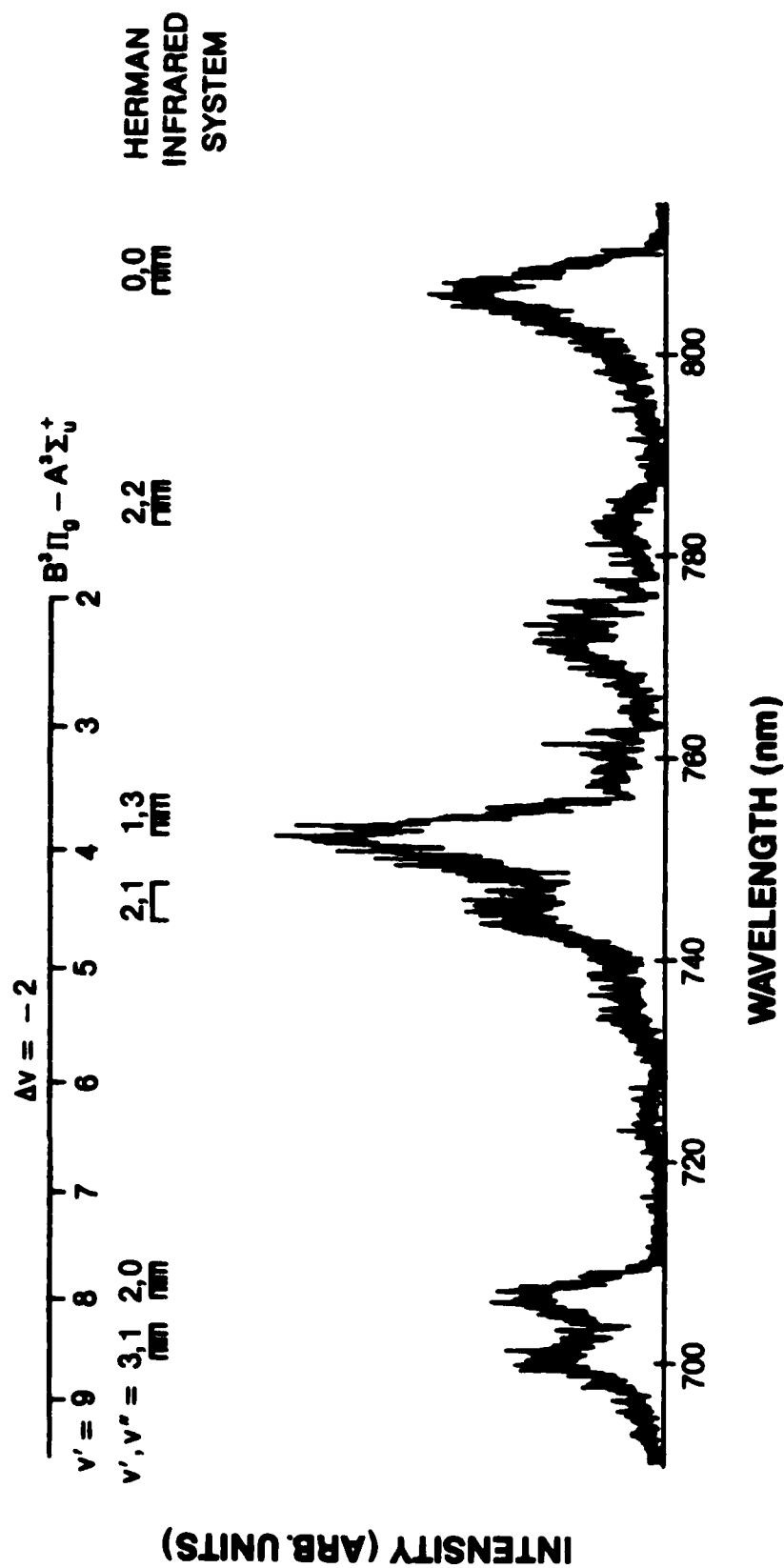
Figure 18. Emission Spectrum in 690 - 815 nm Range of Typical $N_2$ Dielectric-Barrier Discharge.

43
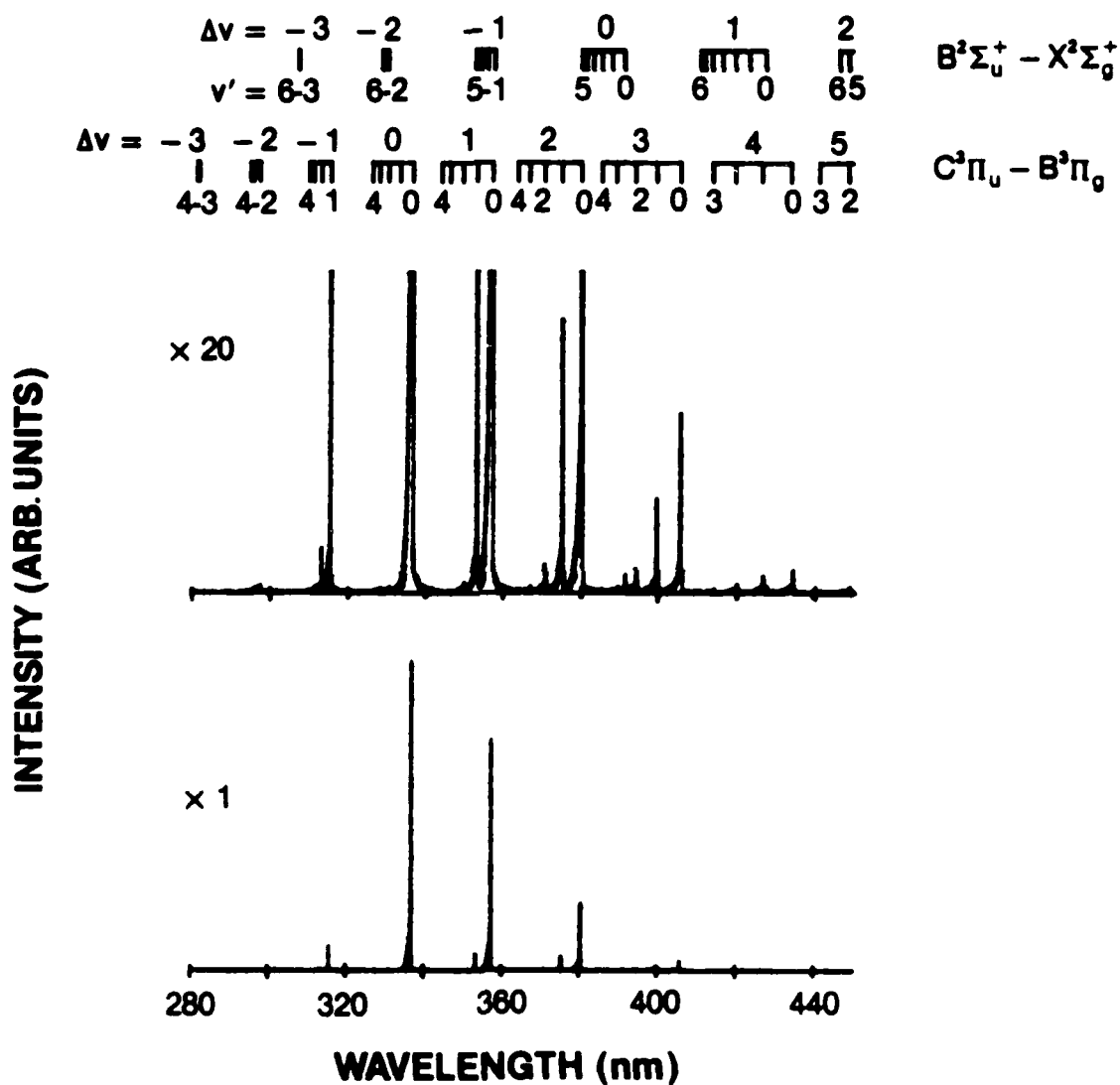
Figure 19. Emission Spectrum in 280 - 450 nm Range of Typical $N_2$ Dielectric-Barrier Discharge.

391.4 nm

$B^2\Sigma_u^+, v' = 0 \rightarrow X^2\Sigma_g^+, v'' = 0$

337.1 nm

$C^3\Pi_u, v' = 0 \rightarrow B^3\Pi_g, v'' = 0$

INTENSITY (ARB. UNITS)

TIME ($\mu$sec)

Figure 20.  Emission-Intensity Waveforms of 200-Torr $N_2$ Dielectric-Barrier Discharge at Downstream Edge of Inner Electrode.  Inner Electrode is Cathode at Time = 0.

45

662.4 nm

$B^3\Pi_g, v' = 6 \rightarrow A^3\Sigma_u^+, v'' = 3$

391.4 nm

$B^2\Sigma_u^+, v' = 0 \rightarrow X^2\Sigma_g^+, v'' = 0$

337.1 nm

$C^3\Pi_u, v' = 0 \rightarrow B^3\Pi_g, v'' = 0$

INTENSITY (ARB UNITS)

TIME ($\mu$sec)

0          200

Figure 21.  Emission-Intensity Waveforms of 200-Torr $N_2$ Dielectric-Barrier Discharge at Center of Downstream Gap.  Inner Electrode is Cathode at Time = 0.

46

391.4 nm

$B^2\Sigma_u^+, v' = 0 \rightarrow X^2\Sigma_g^+, v'' = 0$

337.1 nm

$C^3\Pi_u, v' = 0 \rightarrow B^3\Pi_g, v'' = 0$

INTENSITY (ARB. UNITS)

TIME (μsec)

Figure 22. Emission-Intensity Waveform of 200-Torr $N_2$ Dielectric-Barrier Discharge at Downstream Edge of Outer Electrode. Inner Electrode is Cathode at Time = 0.

As confirmed by others, no evidence of significant N-atom population is found in the discharge. Neither was evidence of significant $N_2(A^3\Sigma_u^+)$ population in the afterglow found. Laser-induced fluorescence (LIF) measurements--discussed in Section V--having a lower detection limit of $\sim 10^{12}$ cm$^{-3}$ of $N_2(A, v = 0)$ gave no indication of $N_2(A)$. 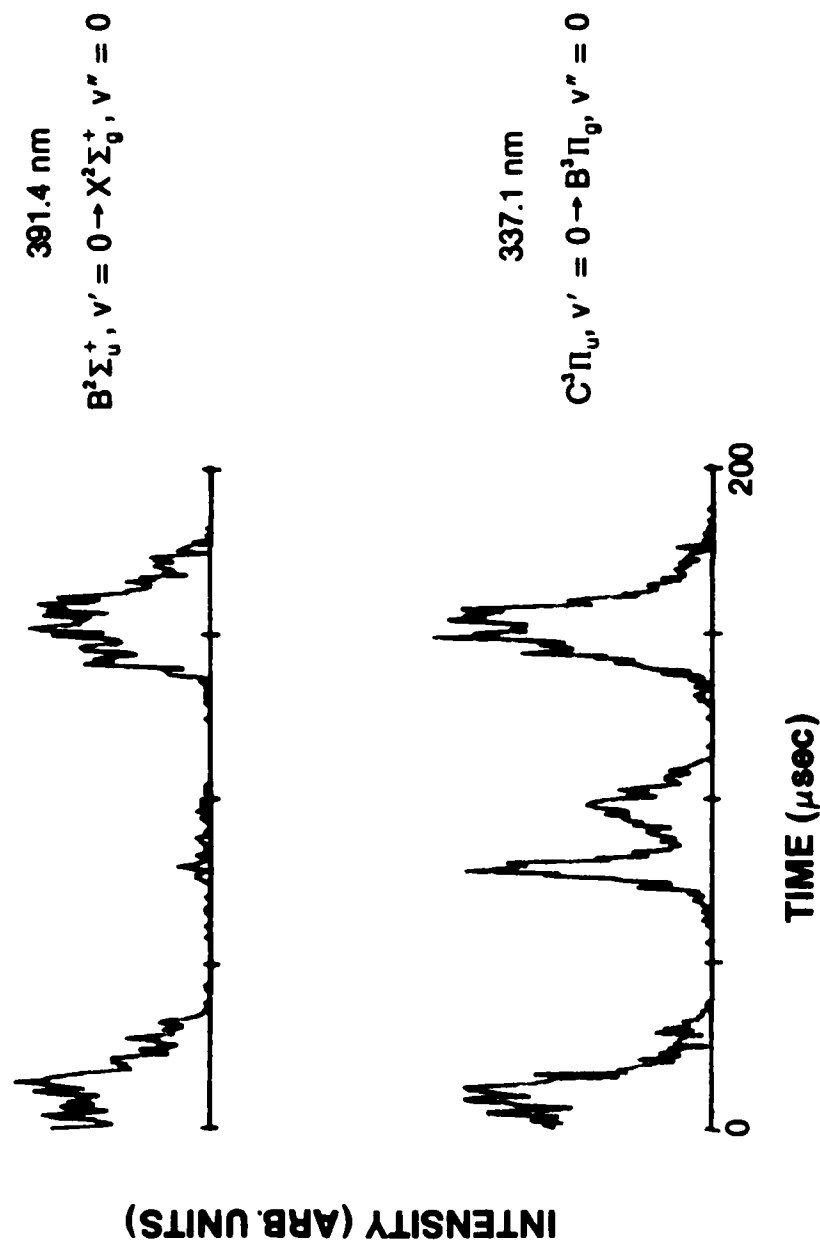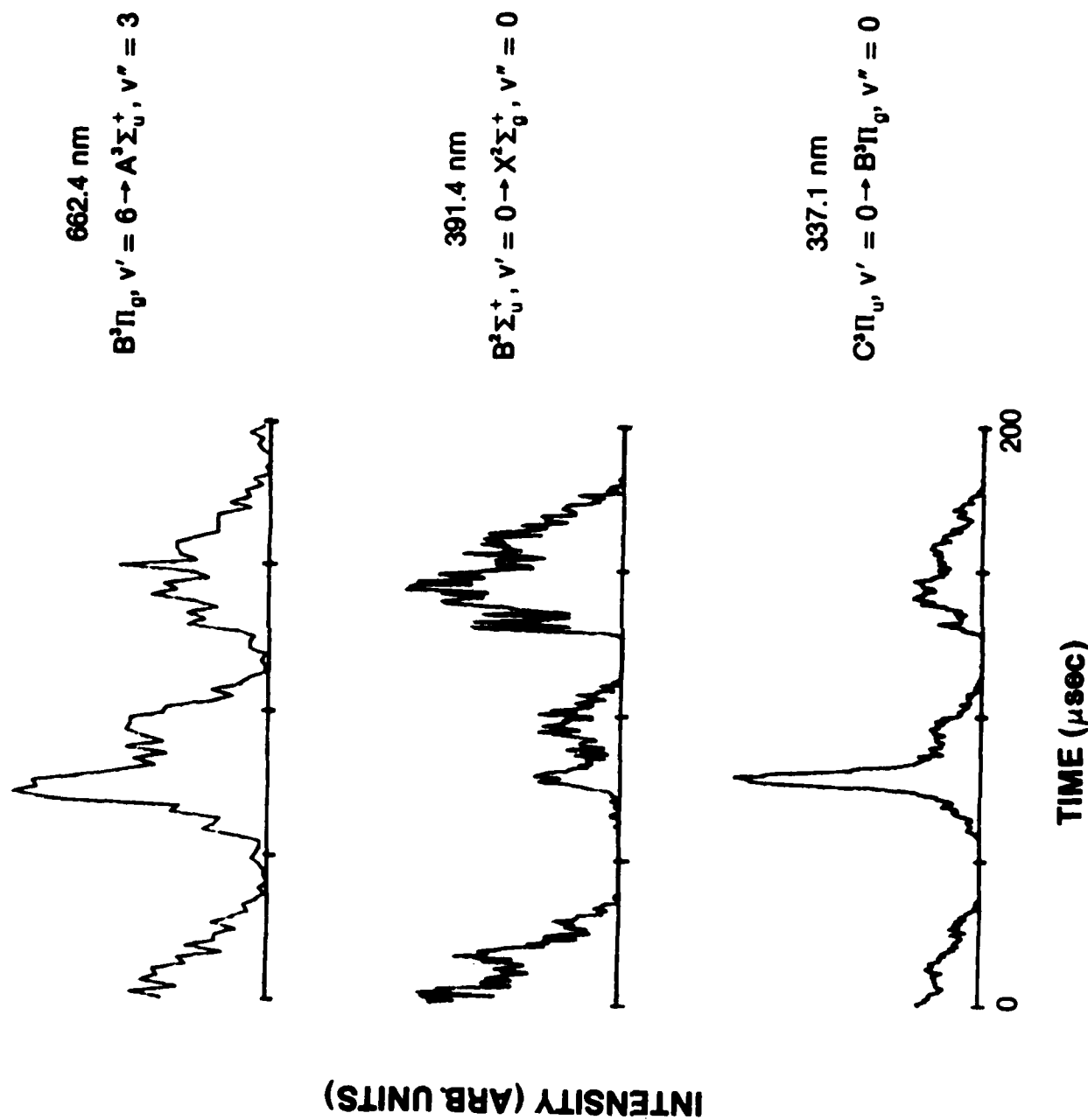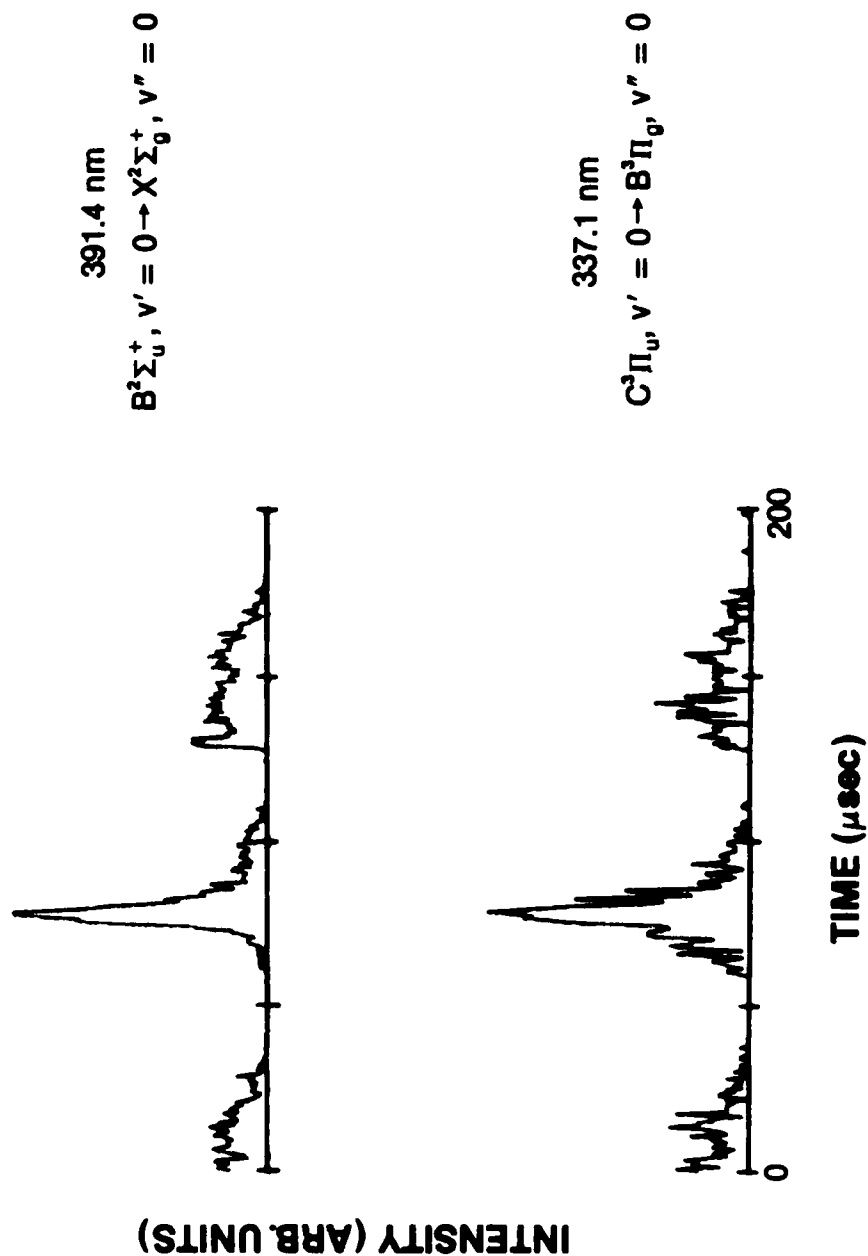Although some second-positive emission is seen in downstream scans, this radiation was found to be temporally synchronized to the discharge emission, indicating that the measurements were merely the result of discharge-emission scattering. Even utilizing the axial afterglow arrangement of Fig. 12 at a flow rate of 3 atm-$\ell$/min., no Vegard-Kaplan emission could be detected; this is in contrast to the careful measurements of Noxon.[16] Unfortunately, the power source limited the power deposition into the discharge to < 40 W average in the present system.

A measurable first-positive spectrum was observed in a dielectric-barrier discharge of Ar, with small quantities of $N_2$ being present. Figure 23 shows the observed spectra in the discharge (downstream end) and in the afterglow (viewed axially in the apparatus of Fig. 11). The Ar pressure was 592.6 Torr, and the $N_2$ pressure was $\sim$ 7.4 Torr (1.2%). The total flow was 2.8 atm-$\ell$/min.

Figure 24 shows the relative populations of the v' levels of the Ar/$N_2$ discharge, calculated by applying measured transition probabilities[2] to the measured intensities of Fig. 23. The populations within the discharge are very similar to those observed by Setser, et al.[61] in measuring the Ar* + $N_2$ energy-transfer reaction in a low-pressure flowing afterglow apparatus. It appears, then, that metastable energy transfer from Ar*($^3P_{2,0}$) occurs in the high-pressure mix within the discharge. The first-positive emission in the high-pressure afterglow, however, is dominated by high v' levels, indicating that N-atom recombination is the source of $N_2(B)$. Visually, the afterglow resembled the Lewis-Rayleigh afterglow.

The afterglow region was searched for the presence of Vegard-Kaplan bands as well as LIF on the $N_2(B \leftarrow A)$ transitions. No evidence of significant $N_2(A)$ could be found.
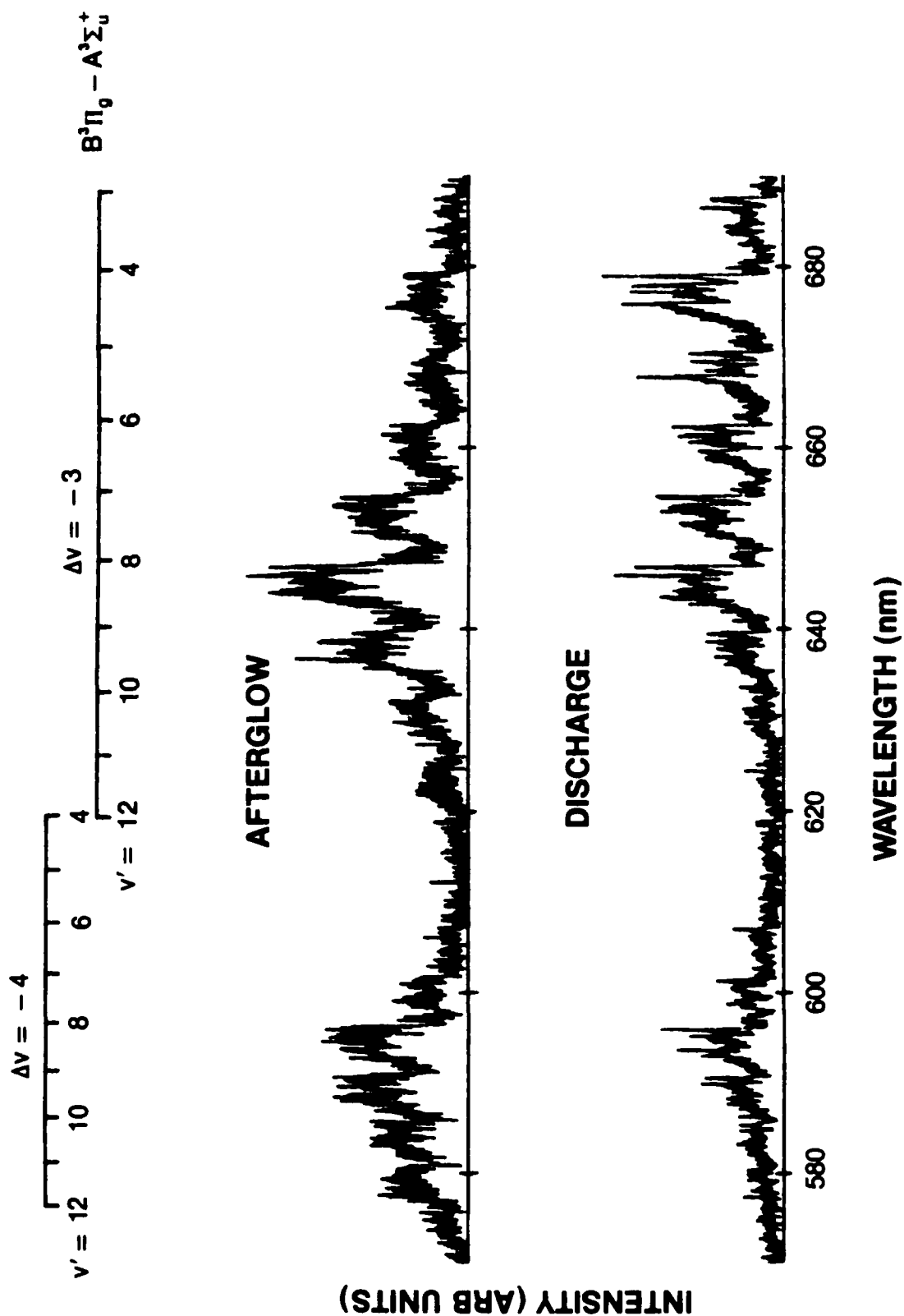
Figure 23.  First-Positive Emission Spectrum of Ar + $N_2$ Dielectric-Barrier Discharge and Afterglow.
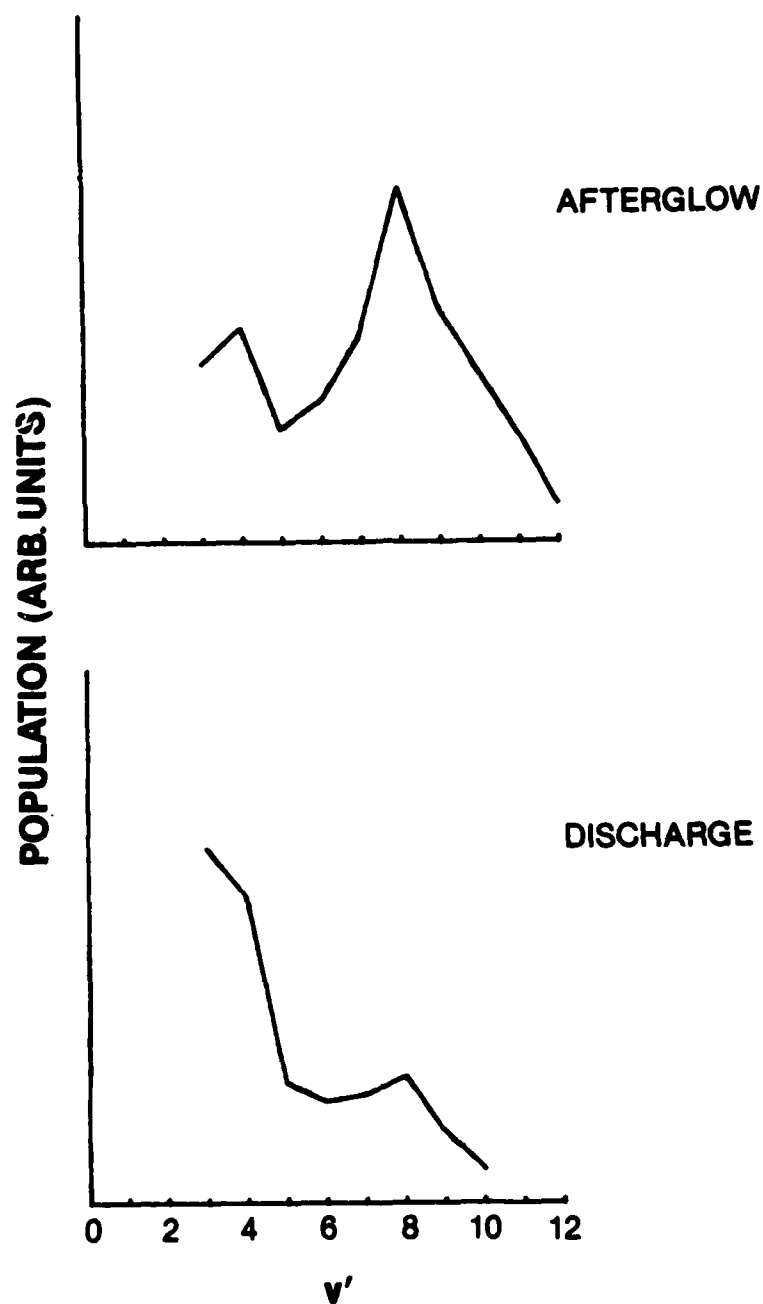
49

Figure 24.  Plot of Relative Populations of Vibrational
Levels of Ar + N2 Dielectric-Barrier Dis-
charge and Afterglow (from Emission Spectrum
of Fig. 23).

## Section V
## DIAGNOSTICS

The major technique used to gather data in the previous sections was emission spectroscopy. Alternative techniques for the detection of $N(^4S)$ and $N_2(A)$ were employed with little success. A discussion of those techniques and their limitations follows.

RAMAN SCATTERING

The possibility of utilizing Raman scattering in measuring the vibrational population of the "pink" afterglow was examined. The number of photons reaching a detector $(E_s)$ resulting from the non-linear Raman process is related to the number density (N) of the probed state by[78]

$$E_s = E_\ell \, \sigma_\ell \, \frac{\nu_\ell}{\nu_s} \, NL\Omega e \tag{6}$$

where $E_\ell$ is the number of laser photons illuminating the detected volume, $\sigma_\ell$ the scattering cross sction, $\nu_\ell$ and $\nu_s$ the optical frequencies of the laser and scattered light, respectively, L the length of the sample in the direction of the laser beam, $\Omega$ the solid angle, and e the optical efficiency of the detection system. The following values apply to the microwave-excited flowing afterglow arrangement:

$$E_s \simeq 10^{17} \text{ photons/pulse (at 600 nm)}$$
$$\simeq 6 \times 10^{17} \text{ photons/pulse (at 308 nm)}$$

$$\sigma_\ell = 2.19 \times 10^{-31} \text{ cm}^2 \text{ ster}^{-1} \text{ mol}^{-1} \text{ (at 600 nm)}$$
$$3.15 \times 10^{-30} \text{ cm}^2 \text{ ster}^{-1} \text{ mol}^{-1} \text{ (at 308 nm)}$$

$$\frac{\nu_\ell}{\nu_s} \simeq 1$$

$$L = 0.5 \text{ cm}$$

$$\Omega = 0.01 \text{ ster}$$

$$e = 0.1\%$$

The values of $\sigma_\ell$ are derived from the measured value[79] of 5.4 x $10^{-31}$ $cm^2$ $ster^{-1}$ $mol^{-1}$ and adjusted for a fourth-power dependence upon frequency.

Assuming a detector (photomultiplier) quantum efficiency of 20%, a signal of one count for every two laser pulses will result from scattering of a 600-nm laser pulse by v = 0 of ground-state nitrogen at atmospheric pressure. This signal is improved to 57 counts/pulse if the 308-nm output of the XeCl laser is used directly. Unfortunately, the detector signal decreases to one count for every five pulses when probing (308 nm) at the 3-Torr pressure of the pink afterglow, and the signals from higher vibrational levels are reduced in proportion to the decrease in number density. Raman scattering is, therefore, not practical for use on the pink-afterglow experimental setup.

Even at the higher pressures of the dielectric-barrier arrangement, the population of v' = 1 would not be expected to exceed $10^{-4}$ times the population of v' = 0. Resulting signal strengths would not be sufficient for reliable measurements in the electrically noisy environment of this discharge.

LASER-INDUCED FLUORESCENCE

The first report of LIF on the $N_2$(B ← A) transitions was in the 1976 work of Heidner, et al.[72] Since that time, the technique has been applied to the study of collisional mixing of the $N_2$ B, B', and W levels.[34,35,37,38,80,81] All of these measurements have been made at pressures of 10 Torr or less and in systems relatively free of first-positive emission. Application of this technique to the low-pressure pink afterglow discussed in Section II proved to be impractical because of the large naturally occurring first-positive radiation. Even in the dark spaces preceding and following the bright-pink glow region, it was not possible to decrease the scatter originating in the pink-glow region sufficiently.

At the higher pressures of the dielectric-barrier afterglow, however, first-positive emission was essentially absent. Also, at these pressures

(200 - 760 Torr), it is expected that the majority of the $N_2(A)$ mole-
cules lie in the $v = 0$ level. Consequently, it was hoped that pumping
on the $N_2(B, v' = 4) \leftarrow (A, v'' = 0)$ transition would result in radiation
from the $(B, v' = 4) \rightarrow (A, v'' = 1)$. However, no LIF was observed.

Three possible explanations for failure to observe LIF are as follows:
1) poor alignment or other factors affecting detection efficiency,
2) rapid collisional quenching of the radiating level, and 3) insuffi-
cient sensitivity of the LIF process to the state being probed.
Although some improvement in detector signal can be expected by install-
ing windowed ports for pumping and viewing, the cylindrical walls of the
afterglow region do not significantly attenuate either pump or fluores-
cence radiation. The most detrimental effect of the tube wall is exces-
sive scatter of the pump beam which may swamp the low-level fluorescence
signal. The 1/2-m Ebert scanning spectrograph was found to be generally
unable to reduce the interference of the scattered pump beam to accept-
able levels. However, the use of a glass cut-off filter in conjunction
with the spectrometer eliminated this interference. The main effect of
the tube walls, then, was imposition of a limit on the power density of
the pump beam; tight focusing would damage the quartz walls.

The major factor affecting detection efficiency of the LIF system was
alignment of the detector optics with the pump region. This problem was
particularly acute when searching for an LIF signal. Originally, the
spectrometer was aligned to the position of maximum scatter of the pump
beam, but this was found to produce unreliable data due to confusion
caused by multiple wall reflections. A method found to be more accept-
able was the use of the Raman-scattered signal in atmospheric-pressure
$N_2$. Through use of a 600-nm pump wavelength, the position of the detec-
tion optics could be adjusted by maximizing the detector signal result-
ing from the 679.6-nm Stokes radiation.

An interesting benefit of the use of the Raman signal for alignment
was an indication of the sensitivity of the fluorescence-measurement
arrangement. As discussed above, the number of photons reaching the
detector ($E_s$) is related to the pump beam ($E_\ell$) by (6). From the

measurements made, one photon was detected for every 1.3 pulses of an ∿ 15-mJ, 17-ns pump pulse, resulting in

$$L\Omega e = 1.4 \times 10^{-6} \text{ cm-ster} \qquad (7)$$

This measurement was made with a 400-μm wide x 2-mm slit opening and a 15-cm lens positioned for one-to-one imaging. Assuming a 0.01-ster viewing angle and a height limited to 1.7 cm by the spectrograph effective aperture ratio of 8.6, the overall system efficiency which could be expected for fluorescence measurements was $1.8 \times 10^{-5}$. That is, one photon will be observed by the photomultiplier for every ∿ 5600 isotropically scattered photons along the pump beam.

The Raman-scattering cross section for the above conditions was ∿ $1.4 \times 10^{-30}$ $cm^2$; the signal was observed at atmospheric pressure. Therefore, if one expects the $N_2(B \leftarrow A)$ single-photon LIF cross section to be on the order of $10^{-17}$ $cm^2$, it would appear that $N_2(A)$ densities on the order of $5 \times 10^6$ $cm^{-3}$ should be detectable with the present arrangement.

Quenching reactions, however, would be expected to decrease the sensitivity of the LIF technique, although collisional quenching reactions of the $N_2(B)$ are not well understood. Vibrational relaxation by $N_2(X)$ would not be expected to be fast since the vibrational-energy spacing of the B-state varies from the spacing of the X-state by more than 700 $cm^{-1}$ at v = 0 and increases with increasing vibrational number.[2] Multiquanta relaxation, invoked to explain the observed relaxation of the A-state and selected levels of the W-state, is also improbable due to large energy separations. However, intersystem crossing of the B-state with the A- and W-states--and, to a lesser extent, with the B'-state-- has been reported by numerous authors. Sedeghi and Setser[35] report a rate coefficient of $1.8 \times 10^{-12}$ $cm^3$ $sec^{-1}$ for transfer of the B, v = 4 into the W-state with Ne bath gas and comment that a larger reaction rate would be expected in pure $N_2$.

54

It appears then that the rate coefficient for collisional quenching of the $N_2$ fluorescing level (B, v' = 4) would be on the order of $10^{-12}$ $cm^3$ $sec^{-1}$ which would result in an effective lifetime of $\sim$ 150 ns at 200 Torr total pressure and only $\sim$ 40 ns at atmospheric pressure. This is a significant reduction when compared to the radiative lifetime of 6.5 $\mu s$. That is, only $\sim$ 2% of the molecules in the upper level will radiate when the pressure is 200 Torr and only $\sim$ 0.6% will decay by radiation at 1 atm.

These numbers will be further reduced when taking the fluorescence branching ratio into account. From measured transition probabilities,[2] $\sim$ 19% of the total radiation of the v' = 4 level will occur on the v' = 4 → v" = 1 transition.

In addition, since $N_2$ is a molecular gas, rotational energy distribution allows only a portion of the vibrational-level population to be pumped; this is a function of gas temperature. From the compiled data of Lofthus and Krupenie,[2] the bandhead of the $N_2$(B, v' = 4) - (A, v" = 0) transition corresponds to the P-branch of J" = 14. At a gas temperature of 300 K, $\sim$ 5% of the molecules in the lower level are in the J" = 13 and 14 for which the P-branch transition energies vary by only 0.01 $cm^{-1}$. Another $\sim$ 5% of the A, v" = 0 molecules lie in the J" = 12 and 15 levels which have P-branch energies which are $\sim$ 0.3 $cm^{-1}$ larger than the J" = 13 and 14 and are separated by 0.04 $cm^{-1}$. If one assumes absorption linewidths of $\sim$ 0.1 $cm^{-1}$ and a pump linewidth of $\sim$ 0.2 $cm^{-1}$, $\sim$ 5 - 7% of the $N_2$(A, v" = 0) molecules are accessible by the probe laser at the P-branch bandhead. At 600 K gas temperature, $\sim$ 7 - 9% of the molecules are in the probe region and $\sim$ 8 - 10% are accessible at 1000 K. The limited linewidth of the absorption, however, will decrease the effective pumping efficiency by $\sim$ 50% for an overall efficiency at room temperature of $\sim$ 2.5 - 3.5%. Reducing the probe linewidth would improve the situation, but use of an etalon in the Lambda-Physik dye laser also reduces the power of the pump beam.

Collisional redistribution of the rotational energy in the upper fluorescing levels (J') may further reduce the LIF efficiency. At room temperature, $\sim$ 8% of the $N_2$(B' = 4) molecules lie in the J' = 11 and 12

(bandhead for $v' = 4 \rightarrow v'' = 1$) levels. However, $\sim$ 50% of the P-branch emission falls within the $\sim$ 0.3-nm linewidth of the spectrograph (400-$\mu$m slit width). If one assumes that approximately one-half of the emission will occur in the P-branch (the other half occurring in the R-branch), then $\sim$ 25% of the upper-level fluorescence should be detectable.

Inaccuracy in wavelength positioning was not a factor. The scanning spectrometer could be tuned to the appropriate wavelength by directing some of the discharge emission to the entrance slit. In addition, wide slit widths (200 - 400 $\mu$m, corresponding to 2.5 - 5 nm FWHM) were generally used, resulting in some forgiveness for a slight wavelength misalignment. The proper wavelength positioning of the Lambda-Physik dye laser (Model 2002, pumped with a Model EMG103MSC Excimer Laser) was determined by inserting an opto-galvanic cell in the dye-laser path. This cell is shown schematically in Fig. 25. By appropriate choice of dye, a rich opto-galvanic spectrum of the B $\leftarrow$ A system was obtained in 3.5 Torr of flowing $N_2$. Although the shape of the opto-galvanic spectrum varied from that reported by Feldmann,[82] the bandhead position (typically triple-peaked) for the needed transitions on the $\Delta v = 4$ sequence was obvious. Generally, the procedure was to set the spectrometer to the emission bandhead peak and then scan the dye laser within the vicinity of the optically determined bandhead peaks. The alternative method was to fix the dye-laser wavelength and scan the spectrometer.

In summary, for the typical conditions of 200-Torr pure $N_2$ at room temperature, $\sim$ 3% of the $N_2(A, v'' = 0)$ molecules can be pumped to the $N_2(B, v' = 4)$ level. Approximately 2% of these molecules will radiate; $\sim$ 19% of the radiation will be on the $v' = 4 \rightarrow v'' = 1$ transition; and $\sim$ 25% of this radiation will fall within the wavelength range of the detector. This results in an overall LIF efficiency of $\sim$ 2.9 x $10^{-5}$. From the Raman signal discussed above, an estimate of the minimum density of the $N_2(A^3\Sigma_u^+, v = 0)$ detectable with the present LIF system is $\sim 10^{11}$ cm$^{-3}$. In addition, it should be pointed out that the Raman scattering signal could be detected only when the dye-laser system was operating at its peak efficiency, with fresh dye and a fresh gas fill in the excimer pump laser. After a day of operation, the dye-laser output
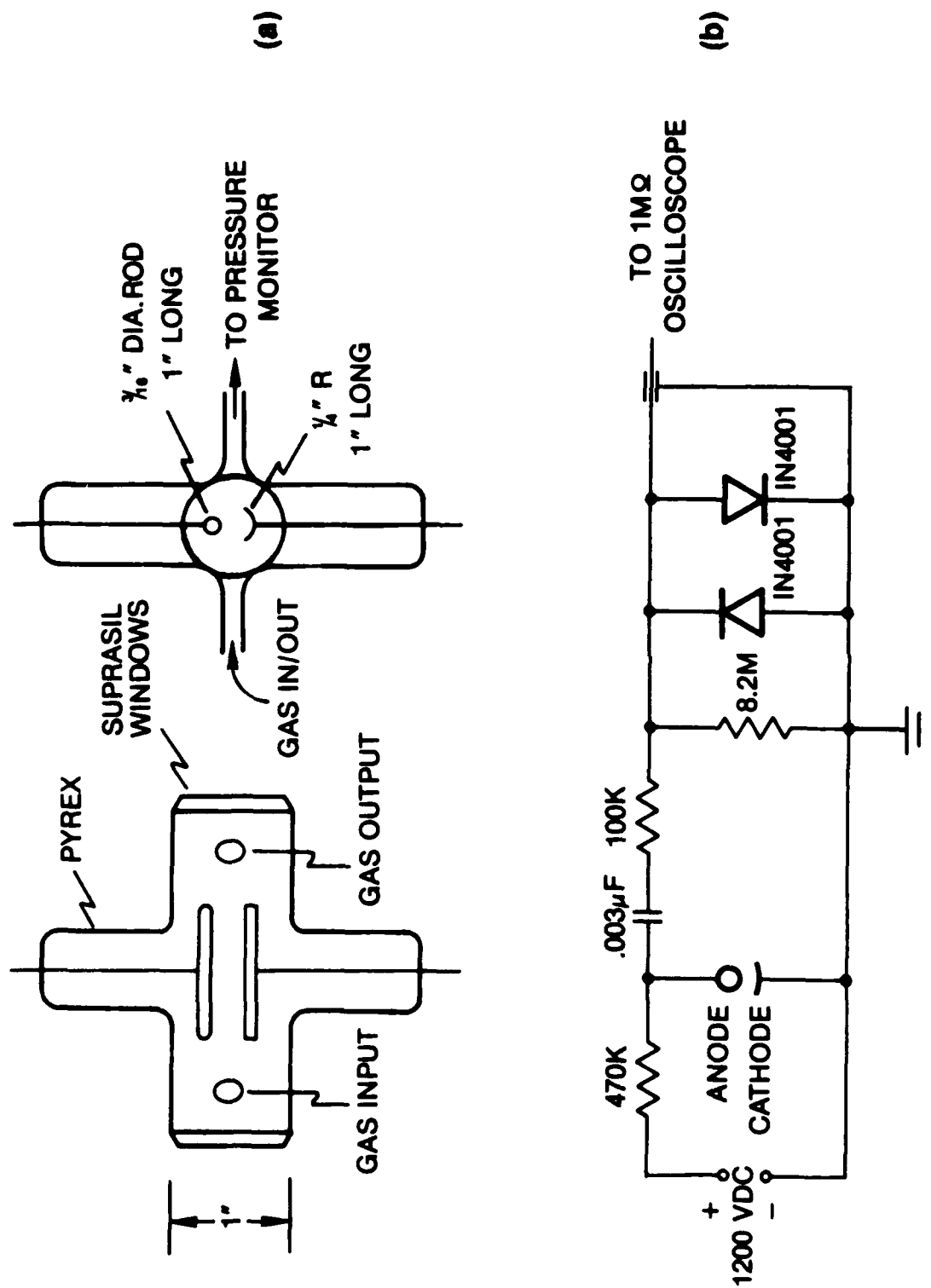
**(a)**

**(b)**

Figure 25. Schematic Diagrams of Opto-galvanic Wavelength Calibration Cell (a)
and Electric Circuit (b).

power had decreased sufficiently that the Raman signal was not clearly discernible. In other words, a more reliable estimate of LIF sensitivity would be $5 - 10 \times 10^{11}$ $cm^{-3}$ at 200-Torr pressure. Because of the increased rate of collisional quenching at increased pressure, the sensitivity at atmospheric pressure is estimated to be no better than $10^{12}$ $cm^{-3}$.
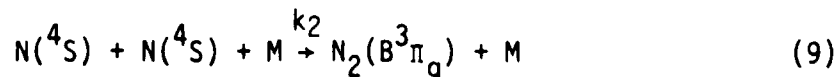
As mentioned above, no LIF on the $N_2(B \leftarrow A)$ system has been detected. It appears likely that the density of $N_2(A)$ in the high-pressure dielectric barrier afterglow system was not sufficient for detection with the existing LIF arrangement. This is consistent with the careful work of Noxon[16] which yielded an afterglow density of $N_2(A)$ of $< 10^{12}$ $cm^{-3}$.

NO TITRATION

Titration of NO as a measurement technique for $N(^4S)$ atom density has been extensively applied.[1] The basic reaction is

$$N(^4S) + NO \overset{k_1}{\rightarrow} N_2 + O \tag{8}$$

with a rate constant[83] $k_8$ of $3.6 \times 10^{-11}$ $cm^3$ $sec^{-1}$. Armstrong, et al.,[56] have demonstrated the applicability of NO titration to calibration of the absolute spectral response of a detection system by observing the decrease of the first-positive emission and the increase of the air-afterglow emission with increasing concentrations of NO. That is, at low pressure the $N_2(B) \rightarrow N_2(A)$ afterglow emission results predominantly from

$$N(^4S) + N(^4S) + M \overset{k_2}{\rightarrow} N_2(B^3\Pi_g) + M \tag{9}$$

followed by

$$N_2(B) \rightarrow N_2(A) + h\nu_1 \text{ (first positive)} \tag{10}$$

where $k_9 = 10^{-32}$ $cm^6$ $sec^{-1}$ (see Refs. 19 and 70) and the radiative lifetime[2] of $N_2(B)$ ranges from 8 $\mu$sec for $v' = 0$ to 4.1 $\mu$sec for $v' = 12$.

In the absence of competing reactions, then, the amount of O-atoms resulting from (8) is proportional to $\sqrt{1/h\nu_1}$. As excess NO is added beyond the titration end point, the air afterglow is observed from

$$O + NO \rightarrow products \rightarrow h\nu \quad (air\ afterglow) \tag{11}$$
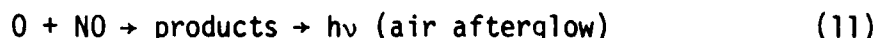
Instrument spectral response can then be calibrated using measured rates[56] for (11).

Unfortunately, limitations of this technique are encountered for pressures $\gtrsim 1.5$ Torr when a pressure dependence is encountered for (11). That is,[84]

$$O + NO + M \rightarrow NO_2^* + M \tag{12}$$

In addition, collisional quenching of $NO_2^*$ becomes a significant interference reaction to (11). It is also conceivable that although the $N_2$ B-state is populated by N-atom recombination, collisional quenching limits the first-positive radiation to levels below the detection limit of the diagnostic system. Therefore, in the absence of first-positive emission at high pressures, NO titration is not applicable as a measurement technique for $N(^4S)$.

In the absence of $N(^4S)$ at high pressures, however, the major source of NO $\gamma$-band radiation should be the result of

$$N_2(A) + NO(X) \rightarrow N_2(X) + NO(A) \tag{13}$$
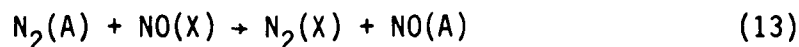
Unfortunately, the very fast radiative lifetime of NO(A) and the complicated mixing pattern within the afterglow tube do not allow a simple relationship among NO-density, $N_2(A)$-density, and NO $\gamma$-band intensity. That is, one NO molecule could effectively radiate many times due to collisions with many $N_2(A)$. In addition, NO diffusion upstream and

subsequent interaction of NO within the discharge field--particularly NO ionization--further complicate the titration mechanism. NO titration techniques are, therefore, of limited use in the high-pressure dielectric-barrier arrangement.

## Section VI
## EXPERIMENTAL EQUIPMENT

Commercially available equipment was utilized for experimental control
and data acquisition whenever possible. For the microwave discharge
studies, spectral recordings were made using standard strip-chart
recording techniques, and a Hewlett Packard Model 320 performed auto-
mated control and recording for the later dielectric-barrier discharge
measurements. A Jarrell Ash model 82-000, 1/2-m Ebert Scanning Mono-
chromator provided the wavelength selectivity, although the motor-drive
mechanism was modified for stepper-motor control (Fig. 26). This con-
trol enabled independent selection of speed and synchronization with a
Linseis Model L4100 Digital Chart Recorder as well as remote control of
the stepper motor by the HP320.

Two photomultipliers were utilized as the photon detectors. An EMI
9659QB with extended S-20 cathode was used in initial microwave after-
glow measurements and in cases where high speed was required. A cooled
Hamamatsu R758, having a Cs-doped GaAs photocathode with fused silica
window, was used in a photon-counting mode for the majority of the
dielectric-barrier-system measurements.

The custom-made power source for the dielectric-barrier discharge is
shown schematically in Figs. 27 (power drivers stage) and 28 (control
logic). This system is essentially an inverter power source utilizing
power MOSFET transistors as switching devices and a step-up transformer
ratio of 67 to achieve the high-voltage output. The discharge is an
integral part of the resonant output circuit; a change in discharge-tube
capacitance would vary the resonant frequency. Variation of the series
inductor (presently 572 $\mu$H) provides the frequency selection.

Photon counting was performed via computer control of a Hewlett-Packard
5334A Universal Counter, with timing controlled through the digital
delay module of Fig. 29. Figure 30 is a schematic diagram of an analog
module, constructed for counter control as well as general timing
requirements. LIF synchronization was provided through the simple LED
detector circuit of Fig. 31. The spectrometer control circuit,
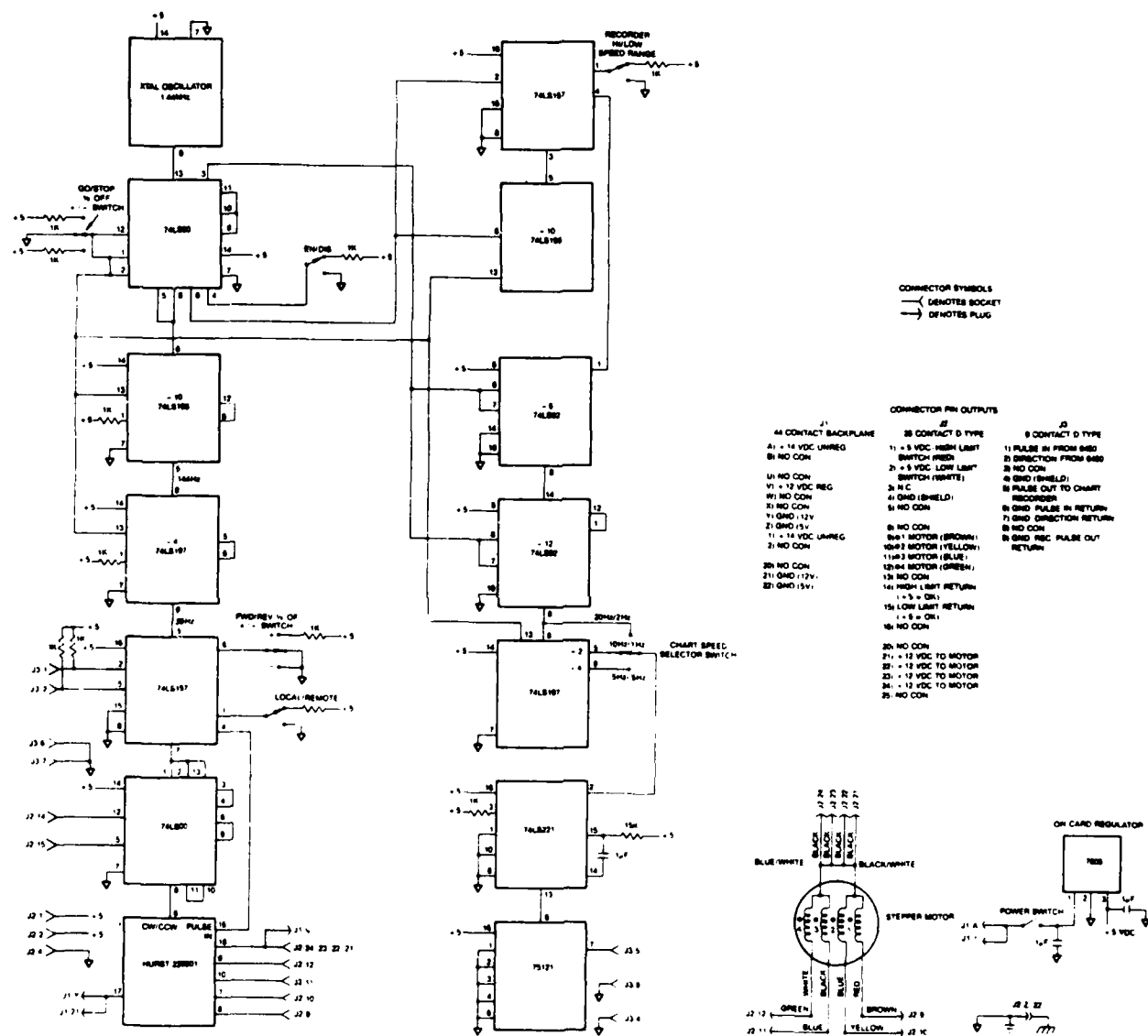
Figure 26. Electrical Schematic of Spectrometer Stepper-Motor Drive Circuit.

Figure 27. Electrical Schematic of Dielectric-Barrier-Discharge Oscillator High-Voltage Section.

63
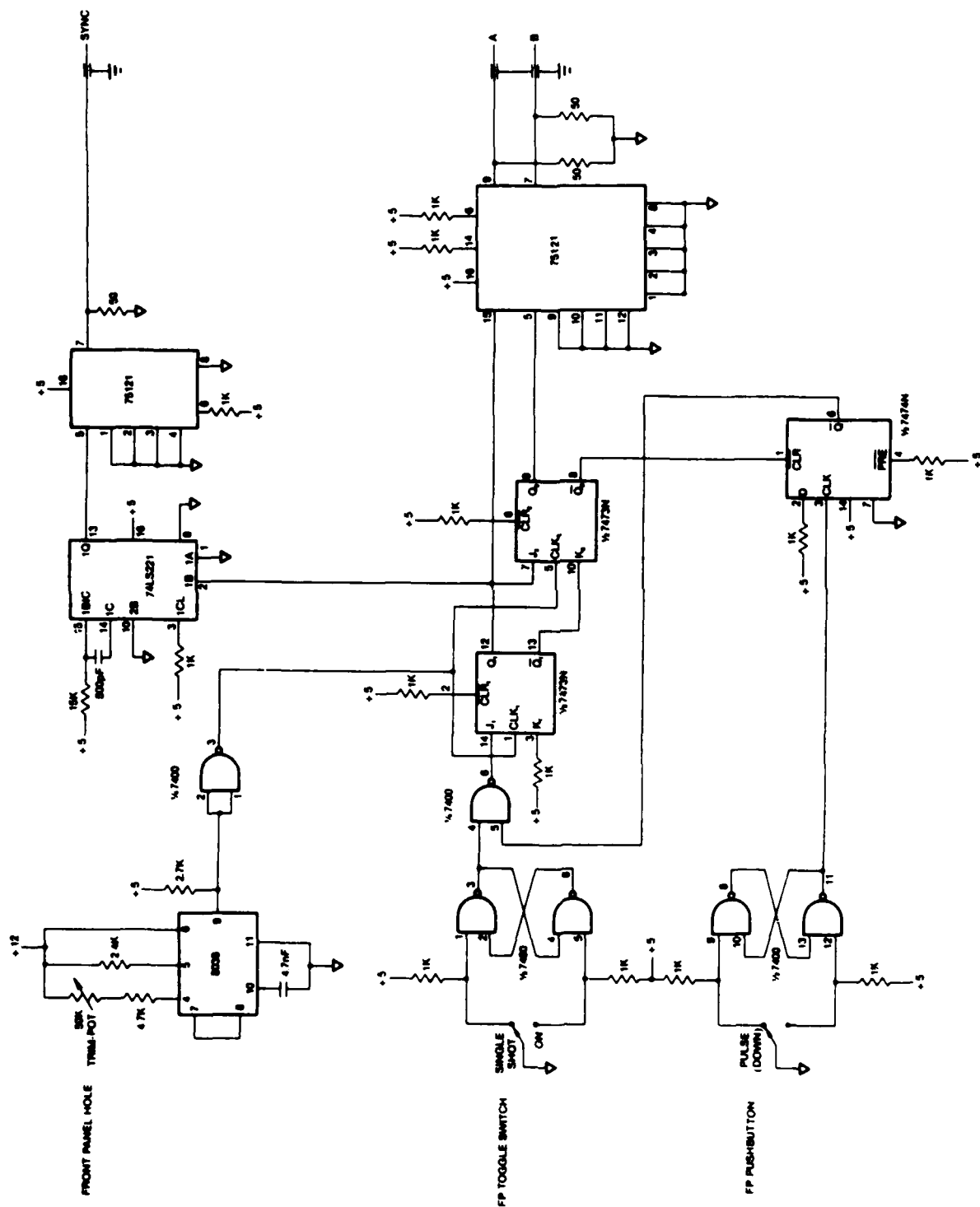
Figure 28. Electrical Schematic of Dielectric-Barrier-Discharge Oscillator Driving Logic.

64
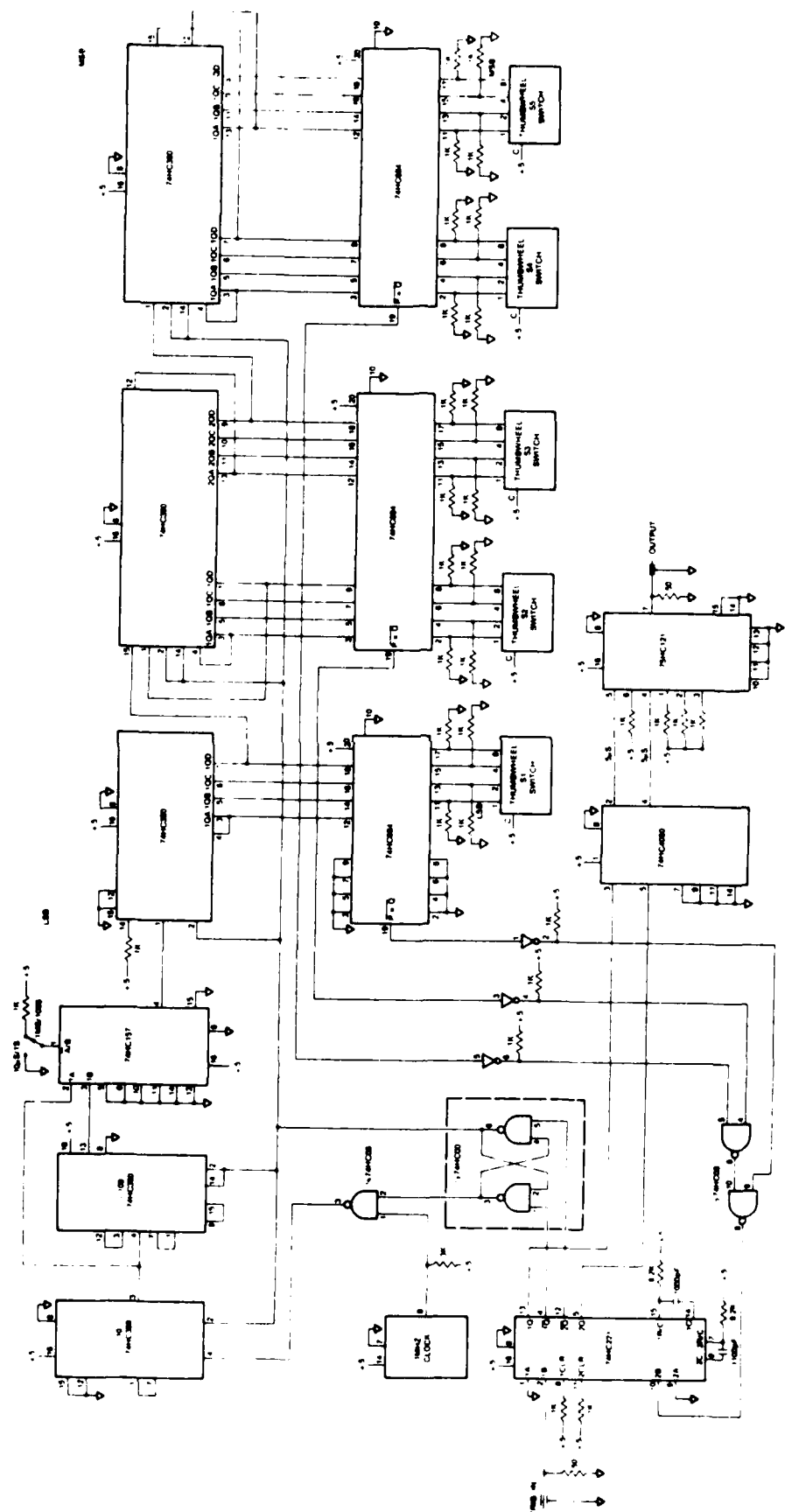
Figure 29. Electrical Schematic of Digital Time-Delay Module.
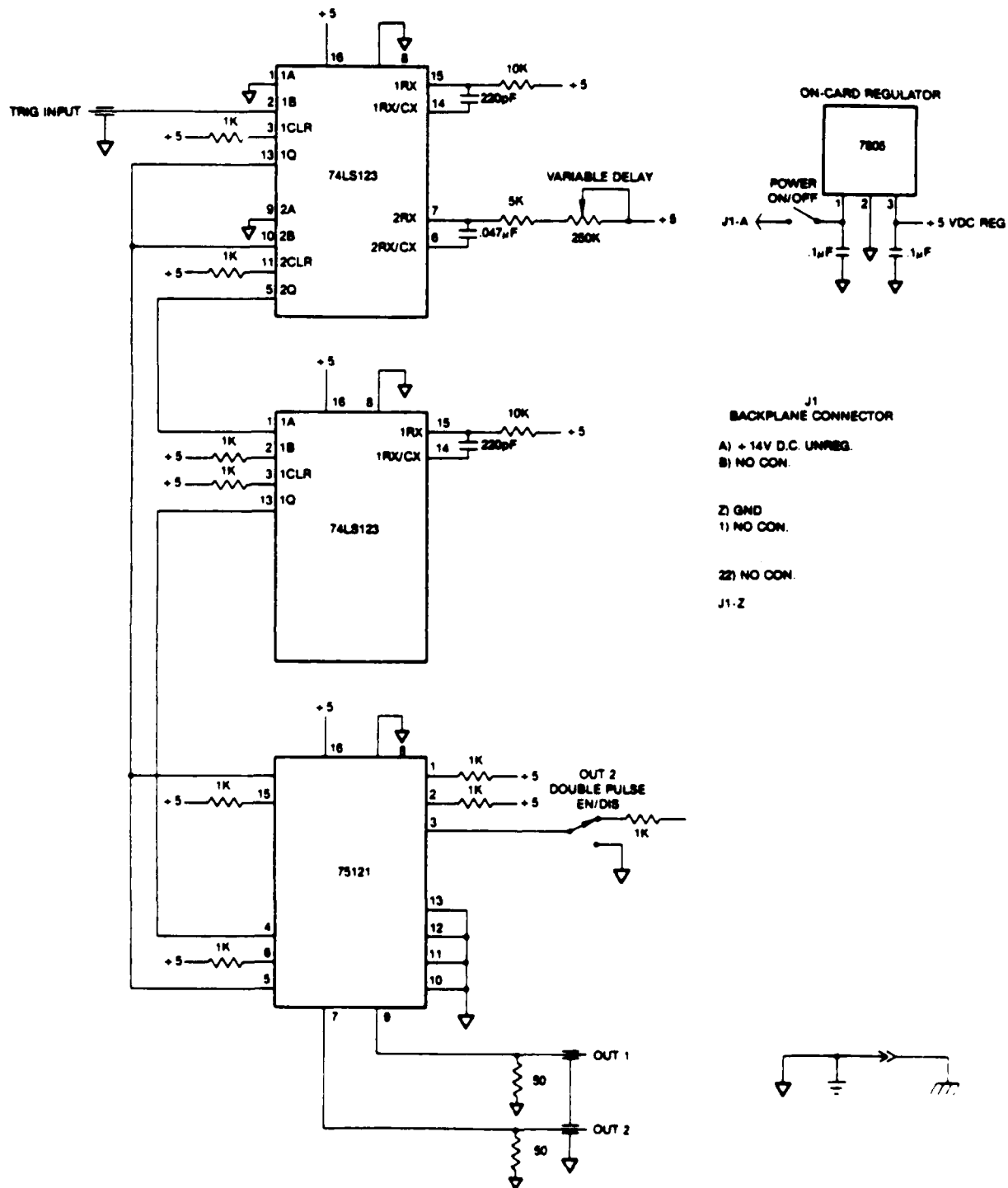
Figure 30. Electrical Schematic of Analog Time-Delay Module.
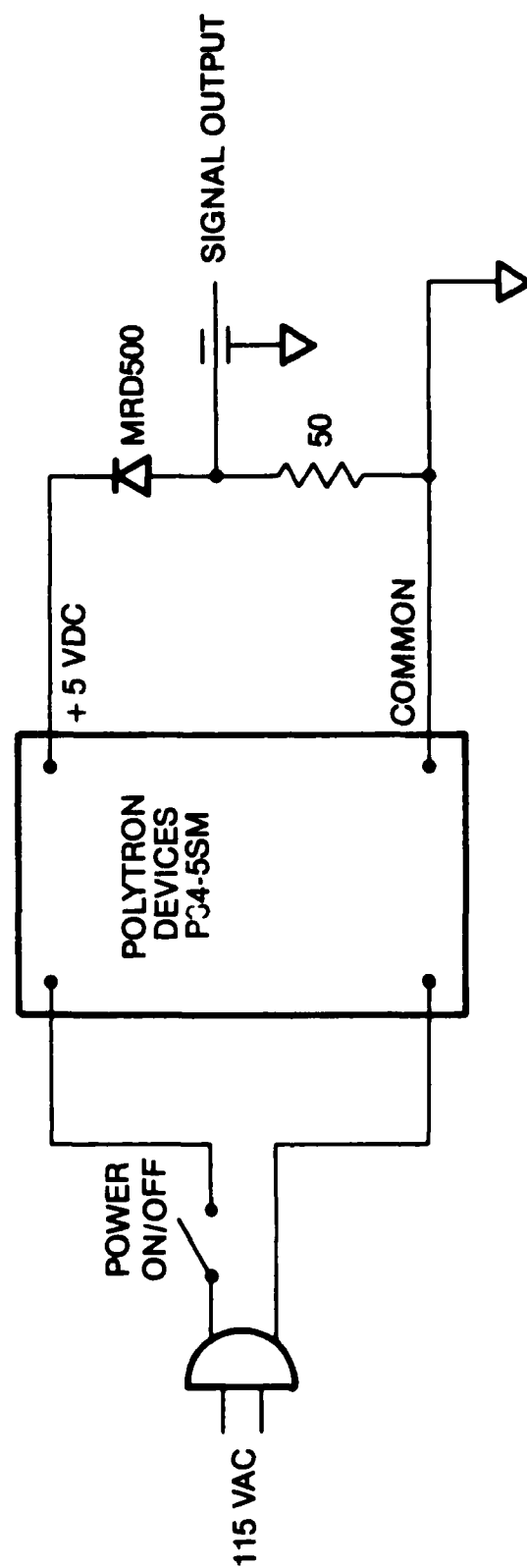
Figure 31. Electrical Schematic of Excimer/Dye-Laser-Output Sync Source.

HV oscillator driving logic, and digital and analog delay modules were constructed in modular form and installed in a rack-mounted cage. Figure 32 is a schematic diagram of the cage power supply.

# D.C. POWER SUPPLY FOR VECTOR MODULE CAGE



Figure 32. Electrical Schematic of Modular-Rack Power Supply.

69

## Section VII
## CONCLUSION

Two electrical-discharge excitation configurations were selected for evaluation as techniques of generating a high density of energetic metastables in flowing, gaseous $N_2$. The surface-wave microwave applicator was promising because of the reported ability to operate at high gas pressures ($\sim$ 1 atm). Also, it was found that this technique could readily produce the highly excited electronic states found in the poorly understood "pink afterglow." The dielectric-barrier discharge, also not well understood, was the second configuration studied. This choice was based upon literature reports of large metastable densities in flowing $N_2$ afterglows.

The microwave technique was found to be incapable of coupling sufficient power to the $N_2$ to effect a discharge at pressures $\gtrsim$ 20 Torr without a buffer gas being present. When Ar was utilized as the buffer gas and the $N_2$ was mixed at a point within the Ar discharge, only the Lewis-Rayleigh afterglow was observed downstream of the discharge region at high pressures. The observed spectral distribution led to the conclusion that $N(^4S)$ atoms were the major source of excited states in the afterglow. Due to the reportedly high quenching reaction rate of N-atoms with $N_2(A^3\Sigma_u^+)$ metastable states, the high-pressure surface-wave technique was judged unacceptable as an excited-state generator.

The low-pressure $N_2$ surface-wave-produced "pink afterglow" was studied briefly. Although electronic states lying > 20 eV above v = 0 of ground-state $N_2$ were observed > 10 msec into the afterglow, the excited state leaving the discharge could not be identified. Considering the low operating pressures necessary for production of this afterglow, the probability of attaining a high density (> $10^{15}$ $cm^{-3}$) of electronically excited states is low. Therefore, the microwave surface-wave technique does not appear feasible as an electrical excitation source of high-density metastables.

Published reports of a high density of the $N_2(A^3\Sigma_u^+)$ in an afterglow of a dielectric-barrier discharge were judged to be erroneously optimistic.

Measurements in this laboratory show the presence of electronically excited states within the discharge region only. No evidence of significant $N_2(A)$ or other excited state could be found in the afterglow using detection techniques with a minimum sensitivitiy to the $N_2(A)$ state of $\sim 10^{12}$ cm$^{-3}$. When Ar buffer gas was utilized with $N_2$, effects were observed indicating that the transfer of energy between the $Ar(^2P)$ metastables and $N_2$ did occur within the discharge; however, the $Ar/N_2$ afterglow was characteristic of a Lewis-Rayleigh afterglow, indicating a large $N(^4S)$ atom density. Therefore, the dielectric-barrier discharge technique was also judged incapable of producing a large population of long-lived excited states in a flowing afterglow configuration.

Although the radiative lifetime of the $N_2(A^3\Sigma_u^+)$ is $\sim 2$ sec., this effort showed that the collisional lifetime at presures of 100 - 760 Torr is much shorter. A great deal of effort is still needed in order to understand the collisional-mixing effects of the myriad of $N_2$ electronic states lying in close energy resonance to each other.

It is concluded that the $N_2(A^3\Sigma_u^+)$ is useful as an energy-transfer intermediary at high densities only if the target species is present within the discharge volume. The only species created in an $N_2$ electrical discharge which is capable of surviving for a significant period of time at significant densities appears to be the $N(^4S)$ atom. It is recommended that future work explore the use of the N-atom as the energy-storage medium.

## REFERENCES

1.  A. N. Wright and C. A. Winkler, <u>Active Nitrogen</u> (Academic Press, New York, 1968).

2.  A. Lofthus and P. H. Krupenie, "The Spectrum of Molecular Nitrogen," J. Phys. Chem. Ref. Data <u>6</u>, 113 (1977).

3.  D. E. Shemansky, "$N_2$ Vegard-Kaplan System in Absorption," J. Chem. Phys. <u>51</u>, 689 (1969).

4.  D. E. Shemansky and N. P. Carleton, "Lifetimes of the $N_2$ Vegard-Kaplan System," J. Chem. Phys. <u>51</u>, 682 (1969).

5.  F. R. Gilmore, "Potential Energy Curves for $N_2$, NO, and $O_2$ and Corresponding Ions," J. Quant. Spectr. Radiat. Transfer <u>5</u>, 369 (1965).

6.  A. B. Callear and P. M. Wood, "Rates of Energy Transfer from $N_2 A^3 \Sigma_u^+$ to Various Molecules," Trans. Faraday Soc. <u>67</u>, 272 (1971).

7.  J. W. Dreyer and D. Perner, "Deactivation of $N_2(A^3\Sigma_u^+, v = 0 - 7)$ by Ground State Nitrogen, Ethane, and Ethylene Measured by Kinetic Absorption Spectroscopy," J. Chem. Phys. <u>58</u>, 1195 (1973).

8.  R. S. T. Chang and R. Burnham., "Dissociative Excitation of $HgBr_2$ by Rare-Gas Metastable Atoms and $N_2(A^3\Sigma_u^+)$," Appl. Phys. Lett. <u>36</u>, 397 (1980).

9.  See, for example, C. M. Ferreira, "Current Research Topics in Low-Pressure Glow Discharges in Rare Gases and in Pure Nitrogen," in <u>Electrical Breakdown and Discharges in Gases</u> (E. E. Kunhardt and L. H. Luessen, Eds.)(Plenum Press, New York, 1983), pp. 395-417 and references therein.

10. D. F. Grosjean, <u>Electric Discharge Excitation and Energy Source Integration</u>, AFWAL-TR-84-2074 (Air Force Wright Aeronautical Laboratories, Wright-Patterson Air Force Base, OH, January 1985).

11. U. Kogelschatz, "Ozone Synthesis in Gas Discharges," XVI International Conference on Phenomena in Ionized Gases - Invited Papers (W. Bötticher and H. W. E. Schulz-Gulde, Eds.)(University of Dusseldorf, Dusseldorf, FRG, 1983), pp. 240-250.

12. M. Hirth, U. Kogenschatz, and B. Eliasson, "The Structure of the Microdischarges in Ozonizers and Their Influence on the Reaction Kinetics," Paper No. C-4-2, Proceedings of the 6th International Symposium on Plasma Chemistry, Montreal, Quebec, Canada, July 1983, pp. 663-66d.

13. C. Heuser and G. Pietsch, "Temporal and Spatial Resolved Photometrical Measurement of the Ozone Concentration in a Model Ozonizer," Paper No. C-4-4, 6th International Symposium on Plasma Chemistry, Vol. 3 (M. I. Boulos and R. J. Munz, Eds.) (International Union of Pure and Applied Chemistry, Montreal, Quebec, Canada, July 1983), pp. 675-680.

14. J. Kishman, E. Barish, and R. Allen, "The Dielectric Discharge as an Efficient Generator of Active Nitrogen for Chemiluminescence and Analysis," Appl. Spectry. 37, 545 (1983).

15. W. B. Dodge and R. O. Allen, "Trace Analysis by Metastable Energy Transfer for Atomic Luminescence," Anal. Chem. 53, 1279 (1981).

16. J. F. Noxon, "Active Nitrogen at High Pressures," J. Chem. Phys. 36, 926 (1961).

17. A. P. D'Silva, G. A. Rice, and V. A. Fassel, "Atmospheric Pressure Active Nitrogen (APAN) - A New Source for Analytical Spectroscopy," Appl. Spectry. 34, 578 (1980).

18. M. F. Golde and B. A. Thrush, "Formation of Excited States of $N_2$ from Ground State Nitrogen Atoms," Faraday Discuss. Chem. Soc. 53, 52 (1972).

19. K. H. Becker, E. H. Fink, W. Groth, W. Jud, and D. Kley, "$N_2$ Formation in the Lewis-Rayleigh Afterglow," Faraday Discuss. Chem. Soc. 53, 35 (1972).

20. J. A. Meyer, D. W. Setser, and D. H. Stedman, "Energy Transfer Reactions of $N_2(A^3\Sigma_u^+)$. II. Quenching and Emission by Oxygen and Nitrogen Atoms," J. Phys. Chem. 74, 2238 (1970).

21. R. A. Young and G. A. St. John, "Experiments on $N_2(A^3\Sigma_u^+)$. I. Reaction with $N_2^*$," J. Chem. Phys. 48, 895 (1968).

22. A. Y. M. Ung, "Observation of the High Vibrational Levels of $N_2(B^3\Pi_g)$ in the Lewis-Rayleigh Afterglow of Nitrogen," J. Chem. Phys. 65, 2987 (1976).

23. M. Moisan, R. Pantel, J. Hubert, E. Bloyet, P. Leprince, J. Marec, and A. Ricard, "Production and Applications of Microwave Surface Wave Plasma at Atmospheric Pressure," J. Microwave Power 14, 57 (1979).

24. V. M. M. Glaude, M. Moisan, and R. Pantel, "Axial Electron Density and Wave Power Distributions along a Plasma Column Sustained by the Propagation of a Surface Microwave," J. Appl. Phys. 51, 5693 (1980).

25. M. Moisan, C. M. Ferreira, Y. Hajlaoui, D. Henry, J. Hubert, R. Pantel, A. Ricard, and Z. Zakrzewski, "Properties and Applications of Surface Wave Produced Plasmas," Rev. Phys. Appl. 17, 707 (1982).

26. M. Moisan, A. Shivarova, and A. W. Trivelpiece, "Experimental Investigation of the Propagation of Surface Waves along a Plasma Column," Plasma Phys. 24, 1331 (1982).

27. M. Moisan, Z. Zakrzewski, R. Pantel, and P. Leprince, "A Waveguide-Based Launcher to Sustain Long Plasma Columns through the Propagation of an Electromagnetic Surface Wave," IEEE Trans. Plasma Sci. PS-12, 203 (1984).

28. J. Delcroix, C. M. Ferreira, and A. Ricard, "Metastable Atoms and Molecules in Ionized Gases," <u>Principles of Laser Plasmas</u> (G. Bekefi, Ed.)(John Wiley and Sons, New York, 1976), p. 162.

29. See D. H. Stedman and D. W. Setser, "Energy Pooling by Triplet Nitrogen $(A^3\Sigma_u^+)$ Molecules," J. Chem. Phys. <u>50</u>, 2256 (1969) and references cited therein.

30. L. G. Piper and G. E. Caledonia, "Rate Constants for Deactivation of $N_2(A^3\Sigma_u^+,\ v' = 0,1)$ by O," J. Chem. Phys. <u>75</u>, 2847 (1981).

31. R. C. Slater, H. A. Hyman, D. Trainor, and A. Flusberg, <u>Research on Sources of Gas Phase Metastable Atoms and Molecules</u>, AFWAL-TR-82-2029 (Air Force Wright Aeronautical Laboratories, Wright-Patterson Air Force Base, OH, May 1982).

32. P. Bletzinger (Air Force Wright Aeronautical Laboratories, Aero Propulsion Laboratory, AFWAL/POOC-3, Wright-Patterson Air Force Base, OH 45433-6563), Private communication.

33. M. F. Golde and B. A. Thrush, "Afterglows," Rep. Prog. Phys. <u>36</u>, 1285 (1973).

34. A. Rotem and S. Rosenwaks, "Laser Induced Fluorescence Studies of Molecular Nitrogen," Opt. Engineering <u>22</u>, 564 (1983).

35. N. Sedeghi and D. W. Setser, "Collisional Coupling and Relaxation of $N_2(B^3\Pi_g)$ and $N_2(W^3\Delta_u)$ Vibrational Levels in Ar and Ne," J. Chem. Phys. <u>79</u>, 2710 (1983).

36. W. Benesch, "Intersystem Collisional Transfer of Excitation in Low Altitude Aurora," J. Chem. Phys. <u>78</u>, 2978 (1983).

37. A. Rotem, I. Nadler, and S. Rosenwaks, "Laser-Induced Fluorescence Studies of Collisional Coupling of $N_2(B^3\Pi_g)$ with $N_2(W^3\Delta)$ and $N_2(A^3\Sigma_u^+)$," Chem. Phys. Lett. <u>83</u>, 281 (1981).

38. N. Sedeghi and D. W. Setser, "Collisional Coupling of $N_2(B^3\pi_g)$ and $N_2(W^3\Delta_u)$ States Studied by Laser-Induced Fluorescence," Chem. Phys. Lett. _77_, 304 (1981).

39. J. Berkowitz, W. Chupka, and G. B. Kistiakowsky, "Mass Spectrometric Study of the Kinetics of Nitrogen Afterglow," J. Chem. Phys. _25_, 457 (1956).

40. I. M. Cambell and B. A. Thrush, "The Recombination of Nitrogen Atoms and the Nitrogen Afterglow," Proc. Roy. Soc. _A296_, 201 (1967).

41. G. E. Caledonia, S. J. Davis, B. D. Green, L. G. Piper, W. T. Rawlins, G. A. Simons, and G. M. Weyl, "Analysis of Metastable State Production and Energy Transfer," AFWAL-TR-86-2078 (Air Force Wright Aeronautical Laboratories, Wright-Patterson AFB, Ohio, November 1986).

42. J. Kaplan, "The Auroral Spectrum," Phys. Rev. _42_, 807 (1932); "A New Band System in Nitrogen," Phys. Rev. _44_, 947 (1933); "New Band System in Nitrogen," Phys. Rev. _45_, 675 (1934); "A New Afterglow System in Nitrogen," Phys. Rev. _48_, 800 (1935).

43. C. R. Stanley, "A New Method for the Production of Active Nitrogen and Its Application to the Study of Collisional Effects in the Nitrogen Molecular Spectrum," Proc. Phys. Soc. _A67_, 821 (1954); "A New Phenomenon Associated with Active Nitrogen," Proc. Phys. Soc. _A68_, 709 (1955).

44. G. E. Beale, Jr., and H. P. Broida, "Spectral Study of a Visible, Short-Duration Afterglow in Nitrogen," J. Chem. Phys. _31_, 1030 (1959).

45. H. P. Broida and I. Tanaka, "Double Probe Measurements of Ionization in Active Nitrogen," J. Chem. Phys. _36_, 236 (1962).

46. A. M. Bass, "Absorption Spectrum of the 'Pink' Afterglow of Nitrogen in the Vacuum Ultraviolet," J. Chem. Phys. $\underline{40}$, 695 (1964).

47. Y. Tanaka, F. R. Innes, A. S. Jursa, and M. Nakamura, "Absorption Spectra of the Pink and Lewis-Rayleigh Afterglows of Nitrogen in the Vacuum-uv Region," J. Chem. Phys. $\underline{42}$, 1183 (1965).

48. R. E. Lund and H. J. Oskam, "The Production and Loss of $N_2^+$ Ions in the Nitrogen Afterglow," Z. Physik $\underline{219}$, 131 (1969).

49. D. Oldenberg, "Mechanism of the Short-Duration Nitrogen Afterglow," J. Opt. Soc. Amer. $\underline{61}$, 1092 (1971).

50. H. H. Brömer and J. Hesse, "Mass Spectrometer Studies of the Ion Composition in the Pink Afterglow," Z. Physik $\underline{219}$, 269 (1969).

51. L. G. Piper and G. E. Caledonia, "Long Lived States in Nitrogen Afterglows," Paper JA-5, 38th Gaseous Electronics Conference, Monterey, California, October 1985.

52. I. M. Campbell and B. A. Thrush, "Some New Vacuum Ultra-violet Emissions of Active Nitrogen," Trans. Farad. Soc. $\underline{65}$, 32 (1969).

53. Designed by M. Andrews, Wright State University, Dayton, Ohio, under contract to the Air Force Wright Aeronautical Laboratories, Aero Propulsion Laboratory (AFWAL/POOC-3), Wright-Patterson Air Force Base, Ohio.

54. J. F. O'Hanlon, A User's Guide to Vacuum Technology (John Wiley and Sons, New York, 1980).

55. M. Chaker and M. Moisan, "Large Diameter Plasma Columns Produced by Surface Waves at Radio and Microwave Frequencies," J. Appl. Phys. $\underline{57}$, 91 (1985).

56. R. A. Armstrong, J. P. Kennealy, F. X. Robert, A. Corman, W. T. Rawlins, L. G. Piper, G. E. Caledonia, B. D. Green, H. C. Murphy, J. I. Steinfeld, R. Stacknik, and S. M. Adler-Golden, "Atmospheric Chemiluminescence: COCHISE and Related Experiments," Report AFGL-TR-82-0305 (Air Force Geophysics Laboratory, Hanscom Air Force Base, MA, 13 October 1982).

57. Y. Tanaka and A. S. Jursa, "A New Method for Producing the Auroral Afterglow of Nitrogen and Its Spectrum," J. Opt. Soc. Amer. 51, 1239 (1961).

58. W. Brennen and M. E. Shuman, "Spectrum of the Lewis-Rayleigh Nitrogen Afterglow," J. Chem. Phys. 66, 4248 (1977).

59. G. H. Hays, C. J. Tracy, A. R. Demonchy, and H. J. Oskam, "Production of $N_2(C^3\pi_u)$ and $N_2(C'^3\pi_u)$ by Mutual Collisions of $N_2(A^3\Sigma_u^+)$ Metastable Molecules," Chem. Phys. Lett. 14, 352 (1972).

60. P. H. Vidaud, R. P. Wayne, M. Yaron, and A. von Engle, "Collisional Quenching of $N_2(A^3\Sigma_u^+; v = 0,1)$ by N Atoms, Ground State $N_2$ and a Pyrex Surface," J. Chem. Soc. London Faraday Trans. II 72, 1185 (1976).

61. D. W. Setser, D. H. Stedman, and J. A. Coxon, "Chemical Applications of Metastable Argon Atoms, IV. Excitation and Relaxation of Triplet States of $N_2$," J. Chem. Phys. 53, 1004 (1970).

62. J. H. Kolts, H. C. Brashears, and D. W. Setser, "Redetermination of the $N_2(C)$ and $N_2(B)$ Branching Ratios from the $Ar(^3P_{0,2})$ + $N_2$ Reaction," J. Chem. Phys. 67, 2931 (1977).

63. V. Puech, F. Collier, and P. Cottin, "Energy Transfer Between Electronically Excited Argon and Nitrogen: A Kinetic Model for the 3371 and 3577 Å Laser Emissions," J. Chem. Phys. 67, 2887 (1977), and references therein.

64. R. W. B. Pearse and A. G. Gaydon, The Identification of Molecular Spectra, Third Edition (John Wiley and Sons, New York, 1963).

65. O. R. Wulf and E. H. Melvin, "Band Spectra in Nitrogen at Atmospheric Pressure. A source of Band Spectra Emission," Phys. Rev. 55, 687 (1939).

66. See, for example, G. Glockler and S. C. Lind, The Electrochemistry of Gases and Other Dielectrics (John Wiley and Sons, New York, (1939).

67. G. A. Capelle and D. G. Sutton, "Analytical Photon Catalysis: Measurement of Gas Phase Concentrations to $10^4/cm^3$," Appl. Phys. Lett. 30, 407 (1977); G. A. Capelle and D. G. Sutton, "Metastable Transfer Emission Spectroscopy - Method and Instrument for Detection and Measurement of Trace Materials in Gas Flows," Rev. Sci. Instrum. 49, 1134 (1978); J. E. Melzer, J. L. Jordan, and D. G. Sutton, "Determination of Trace Amounts of Lead in Water by Metastable Transfer Emission Spectrometry," Anal. Chem. 52, 348 (1980).

68. W. B. Dodge, III, and R. O. Allen, "Trace Analysis by Metastable Energy Transfer for Atomic Luminescence," Anal. Chem. 53, 1279 (1981).

69. G. W. Rice, J. J. Richard, A. P. D'Silva, and V. A. Fassel, "Atmospheric Pressure Active Nitrogen Afterglow as a Detector for Gas Chromatography," Anal. Chem. 53, 1519 (1981).

70. W. Brennen and E. C. Shane, "The Nitrogen Afterglow and the Rate of Recombination of Nitrogen Atoms in the Presence of Nitrogen, Argon, and Helium," J. Phys. Chem. 75, 1552 (1971).

71. J. W. Dreyer and D. Perner, "The Deactivation of $N_2$ $B^3\Pi_g$, v = 0 - 2 and $N_2$ $a'^1\Sigma_u^-$, v = 0 by Nitrogen," Chem. Phys. Lett. 16, 169 (1972).

72. R. J. Heidner, III, D. G. Sutton, and S. N. Suchard, "Kinetic Study of $N_2(B^3\Pi_g, v)$ Quenching by Laser-Induced Fluorescence," Chem. Phys. Lett. <u>37</u>, 243 (1976).

73. W. Benesch and D. Fraedrich, "The Role of Intersystem Collisional Transfer of Excitation in the Determination of $N_2$ Vibronic Level Populations. Application to $B'^3\Sigma_u^- - B^3\Pi_g$ Band Intensity Measurements," J. Chem. Phys. <u>81</u>, 5367 (1984).

74. M. A. Bagirov, K. S. Burziev, and M. A. Kurbanov, "Characteristics of a Low-Pressure Discharge in Air Between Dielectrics," Zh. Tekh. Fiz. <u>49</u>, 339 (1979).

75. C. Heuser and G. Pietsch, "Temporal and Spatial Resolved Photometrical Measurements of the Ozone Concentration in a Model Ozonizer," Paper C-4-4, Presented at the 6th International Symposium on Plasma Chemistry, Montreal, July 1983.

76. Nanochem Purifier System, 0.3 Liter, purchased from Hercules, Inc., Marketing Center, Wilmington, DE 19899.

77. P. K. Wittman and J. W. Mitchell, "Ultrapurification of Nitrogen Monitored by Metastable Transfer Emission Spectroscopy," Appl. Spectry. <u>40</u>, 156 (1986).

78. R. Goulard, "Laser Raman Scattering Applications," in <u>Laser Raman Gas Diagnostics</u> (M. Lapp and C. M. Penny, Eds.) (Plenum Press, New York, 1974), pp. 3-14.

79. H. A. Hyat, J. M. Cherlow, W. R. Fenner, and S. P. S. Porto, "Cross Section for the Raman Effect in Molecular Nitrogen Gas," J. Opt. Soc. Amer. <u>63</u>, 1604 (1973).

80. J. M. Cook, T. A. Miller, and V. E. Bondybey, "Laser Induced Fluorescence Detection and Characterization of Ionic and Metastable Reaction Products," J. Chem. Phys. <u>69</u>, 2562 (1978).

81. A. Rotem, I. Nadler, and S. Rosenwaks, "Direct Observation of Collision Induced Transitions from $N_2(B^3\pi_g)$ to $N_2(B'^3\Sigma_u^-)$," J. Chem. Phys. <u>76</u>, 2109 (1982).

82. D. Feldman, "Opto-Galvanic Spectroscopy of Some Molecules in Discharges: $HN_2$, $NO_2$, $H_2$ and $N_2$," Opt. Commun. <u>29</u>, 67 (1979).

83. M. A. A. Clyne and B. A. Thrush, "Kinetics of the Reactions of Active Nitrogen with Oxygen and with Nitric Oxide," Proc. Roy. Soc. <u>A261</u>, 259 (1961). See also Ref. 56 and references therein.

84. K. H. Becker, W. Groth, and D. Thron, "The Mechanism of the Air-Afterglow $NO + O \rightarrow NO_2 + h\nu$," Chem. Phys. Lett. <u>15</u>, 215 (1972).

END

10-81

DTIC